machines

MDPI

Article

Guiding the Selection of Multi-Vector Model Predictive Control Techniques for Multiphase Drives

Juan Jose Aciego, Ignacio Gonzalez-Prieto *, Mario Javier Duran, Angel Gonzalez-Prieto and Juan Carrillo-Rios

Electrical Engineering Departament, Industrial Engineering School, University of Malaga, 29010 Malaga, Spain; juanjoseaciego@uma.es (J.J.A.); mjduran@uma.es (M.J.D.); anggonpri@uma.es (A.G.-P.); juan.carrillo.rios@uma.es (J.C.-R)

* Correspondence: igp@uma.es

Abstract: A diverse group of so-called multi-vector techniques has recently appeared to enhance the control performance of multiphase drives when a direct control strategy is implemented. With different numbers of switching states and approaches for estimating the application times, each multi-vector solution has its own nature and merits. Previous studies have individually tested each version of the proposed finite-control-set model predictive control (FCS-MPC) strategies using a single experimental setup with specific parameters and, in some cases, using a limited range of operating conditions and focusing exclusively on some control aspects. Although such works provide partial contributions, the control performance is highly affected by the test and rig conditions, being dependent on the machine parameters, the switching frequency and the range of operation. Consequently, it becomes difficult to extract some universal conclusions that guide the control designer on the best alternative for each application. Aiming to enrich the knowledge in this field and provide a broader picture, this work performs a global analysis with different multi-vector techniques, various machine parameters, multiple operating points and a complete set of indices. Experimental results confirm that the selection of the most adequate control strategy is not a trivial task because the degree to which multi-vector techniques are affected by the test conditions is variable and complex. Some tables with a qualitative analysis, based on the extensive empirical tests, contribute with a more complete insight and guide eventual control designers on the decision about the optimal regulation approach to be chosen.

Keywords: finite-control-set model predictive control; multiphase electric drives; multi-vector assessment; multi-vector guiding selection

check for updates

Citation: Aciego, J.J.; Gonzalez-Prieto, I.; Duran, M.J.; Gonzalez-Prieto, A.; Carrillo-Rios, J. Guiding the Selection of Multi-Vector Model Predictive Control Techniques for Multiphase Drives. *Machines* **2024**, *12*, 115. https://doi.org/10.3390/machines12020115

Received: 11 December 2023
Revised: 22 January 2024
Accepted: 1 February 2024
Published: 7 February 2024

Copyright: © 2024 by the authors. Licensee MDPI, Basel, Switzerland. This article is an open access article distributed under the terms and conditions of the Creative Commons Attribution (CC BY) license (https://creativecommons.org/licenses/by/4.0/).

1. Introduction

A global energetic transition is necessary to safeguard the future of our planet. Since the Earth can only regenerate resources at a finite rate, the sustainable usage of the available energetic resources should be assumed as a mandatory task for the present-day society. Focusing on the case of electrical energy, the role of electric drives is currently key in the electromechanical energy conversion process. In this context, multiphase electric drives are an interesting choice for variable-speed industrial applications with more demanding requirements [1,2] because they offer an enhanced fault tolerance and a reduced per-phase current rating without increasing the rated voltage [3–5]. The first advantage is related to the reliability, whereas the second one is crucial from the perspective of the system losses. These features can be assumed as essential requirements for the new generation of electric drives in the aforementioned energetic transition.

Control designers and research groups have explored diverse trends of regulation techniques to take advantage of the multiphase electric drive abilities [6–8]. There are different criteria to classify the available control schemes, for instance, according to how they generate the gate signals. In this regard, the regulation algorithms can be categorized

as control methods with a pulse-width modulation (PWM) stage or direct control strategies. In the case of the first family of controllers, indirect-rotor-field-oriented control (IRFOC) has merited special attention due to its suitable robustness and high-quality current [9,10]. Nevertheless, this popular regulation technique also shows some limitations related to the dc-link voltage usage [11] or the inclusion of additional control restrictions [12,13]. Fortunately, the efforts of the research community permitted the mitigation of the mentioned limitations. For example, the development of different overmodulation algorithms has allowed for a higher dc-link voltage utilization of linear controllers [14–17] and, consequently, a faster dynamic response. Concerning direct regulation techniques, model predictive control (MPC) has appeared as an attractive solution for exploiting the inherent advantages of multiphase electric drives. The flexibility of this approach has been employed to add, in a simple manner, some extra control goals [18–20]. For example, refs. [19,21] proposed the usage of adaptive and tunable cost functions to improve current quality and [20] promoted the reduction in the common-mode voltage thanks to the MPC nature. In addition, MPC schemes achieve a higher dc-link usage without the inclusion of any additional overmodulation algorithm. This fact permits obtaining a better dynamic response if the conventional versions of both control techniques are employed. However, MPC based on the application of a single switching state per control period presents an unacceptable current quality. Fortunately, this undesirable harmonic content has been mitigated with the development of multi-vector solutions [22–33]. In fact, ref. [27] illustrated a substantial improvement in terms of current quality thanks to the development of multi-vector control actions. The proposed implicit modulation stage achieved a notable reduction in the secondary components, providing a better current quality than in the case of the conventional carrier-based PWM technique.

Regardless of the selected family of controllers, it can be concluded that the last decade has witnessed success, where a high number of more competitive control techniques have been developed in diverse application fields such as renewable energy application [34] or electrical propulsion [35,36]. The most popular procedure in the field of electric drives to illustrate the goodness of an original proposal of the state of the art is an experimental comparison using a benchmark method as a basis for the verification [23–33,37,38]. Focusing on the necessary validation process, it is also common to carry out the mentioned comparison on a single test bench where the electric machine is characterized by specific values of its electrical parameters [18,20,22–27,31]. Taking into account this last issue, a reasonable doubt can appear regarding the universality of the obtained conclusions. For instance, from the perspective of the signal quality in multiphase drives, the role of the secondary currents (x-y components) is crucial [27,33,39–41], and the behavior of these components is highly dependent on the stator parameters [42,43]. In this regard, the implementation of a multi-vector solution can be considered as a mandatory task when a direct control strategy is implemented to regulate multiphase electrical machines with low values of the stator impedance. The effectiveness of this control solution has also been confirmed in three-phase drives when the current quality is assumed as the main control target [44–47]. However, if the machine shows a high value of the equivalent stator impedance, the utilization of a multi-vector voltage output may not be required if some additional control goals, such as low switching frequency, are also considered. On the other hand, although the electric drive is formed by an electrical machine and a voltage source converter (VSC), it is common to focus the analysis on the machine [24,26,27,48,49]. Unfortunately, assuming this approach, the proposed analysis is blind to the global performance of the system [50].

Based on the aforementioned limitations, this work introduces a generalized analysis where four different multi-vector MPC strategies are compared in diverse configurations of a six-phase induction machine for different operating conditions. Considering the goal of this proposal, some decisions have been taken in order to ensure a suitable level of universality. For instance, focusing on the considered implicit modulation stages, since the purpose of this work is to carry out a more generalized analysis, the multi-vector solutions have been selected in order to obtain a wide range of control approaches. In this way, in the selected schemes, the voltage outputs are composed of a different number

and/or type of voltage vectors (Table 1), the estimation of active duty cycles is performed based on an offline or online process and the mitigation of the secondary currents has been addressed from different perspectives. On the other hand, the employed electric drive has been modified to obtain different values of the stator electrical parameters. The extensive experimental results permit evaluating the system performance from different perspectives. Firstly, the signal quality has been studied using the total harmonic distortion and the peak-to-peak value of the secondary currents as quality indices. The tracking of the reference currents has also been monitored in this study. This analysis allows for observing, in an indirect form, the usage of the dc-link voltage for each multi-vector solution. In addition, the impact of these algorithms on the VSC performance has also been quantified using, for that purpose, the VSC power losses as a basis of comparison.

This study has been designed using analytical and experimental perspectives. In this work, the control designer can obtain a global view of how the control scheme performance may be affected depending on the available electric drive and the application requirements. Two overview tables have been included, where the future control designers can obtain, in a qualitative manner, interesting information about the main advantages of the considered strategies. Finally, it is important to highlight that this work aims to emphasize the need for using diverse test benches to obtain generalized conclusions about the performance of a proposed control scheme.

Table 1. Selected multi-vector solutions.

Ref.	Acronym	Nature	Switching States per Control Action	Null-Avg x-y Volt.	Inst. x-y Harm.
[26]	VV-MPC	Offline	2	✓	✗
[25]	LVV-MPC	Offline	2	✗	✓
[24]	PULLA-MPC	Online	3	✓	✓
[27]	MV5-MPC	Online	5	✓	✓

2. Six-Phase Electric Drives: Generalities and Topology

In this work, a multiphase electric drive is employed. Specifically, the selected one is formed by an asymmetrical six-phase induction machine (6PH-IM) supplied by a dual two-level three-phase voltage source converter (2L-VSC). Regarding the 6PH-IM, it is composed of two sets of three-phase windings. These stator windings are distributed and spatially shifted 30° and each three-phase set has a star connection with independent neutral points. The use of two isolated neutral points permits simplifying the regulation schemes. As shown in the topology included in Figure 1, each three-phase winding set is fed exclusively by a 2L-VSC. Moreover, both 2L-VSCs are connected to a single dc-link.

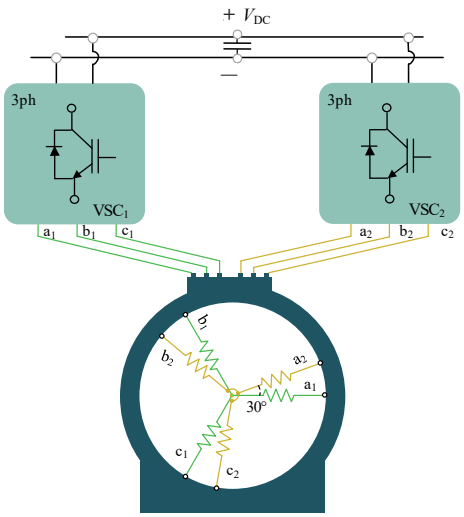


Figure 1. Asymmetrical six-phase electric drive topology.

The state of each VSC leg can be defined as S_i, where $S_i = 0$ if the lower switch is ON and the upper one is OFF, and $S_i = 1$ if the opposite happens. This VSC configuration provides 64 voltage outputs (2^6). It is possible to express all available switching states as a vector $[S] = [S_{a1}S_{b1}S_{c1}S_{a2}S_{b2}S_{c2}]$, where each component defines the conduction state of each converter leg. Every stator phase voltage (v_{si}) can be obtained using the available switching states $[S]$ and the dc-link voltage (V_{DC}) as expressed in (1).

$$\begin{bmatrix} v_{a1} \\ v_{b1} \\ v_{c1} \\ v_{a2} \\ v_{b2} \\ v_{c2} \end{bmatrix} = \frac{V_{DC}}{3} \begin{bmatrix} 2 & -1 & -1 & 0 & 0 & 0 \\ -1 & 2 & -1 & 0 & 0 & 0 \\ -1 & -1 & 2 & 0 & 0 & 0 \\ 0 & 0 & 0 & 2 & -1 & -1 \\ 0 & 0 & 0 & -1 & 2 & -1 \\ 0 & 0 & 0 & -1 & -1 & 2 \end{bmatrix} \begin{bmatrix} S_{a1} \\ S_{b1} \\ S_{c1} \\ S_{a2} \\ S_{b2} \\ S_{c2} \end{bmatrix}. \tag{1}$$

In this field of work, the use of different references frames and matrix transformations is widely extended to ease the understanding and regulation of the multiphase electric drives. Among them, vector-space decomposition (VSD) is the most popular approach in the field of multiphase electric drives [51]. Using the amplitude-invariant Clarke transformation (2), it is possible to express phase variables onto three orthogonal subspaces.

$$[C] = \frac{1}{3} \begin{bmatrix} 1 & -\frac{1}{2} & -\frac{1}{2} & \frac{\sqrt{3}}{2} & -\frac{\sqrt{3}}{2} & 0 \\ 0 & \frac{\sqrt{3}}{2} & -\frac{\sqrt{3}}{2} & \frac{1}{2} & \frac{1}{2} & -1 \\ 1 & -\frac{1}{2} & -\frac{1}{2} & -\frac{\sqrt{3}}{2} & \frac{\sqrt{3}}{2} & 0 \\ 0 & -\frac{\sqrt{3}}{2} & \frac{\sqrt{3}}{2} & \frac{1}{2} & \frac{1}{2} & -1 \\ 1 & 1 & 1 & 0 & 0 & 0 \\ 0 & 0 & 0 & 1 & 1 & 1 \end{bmatrix}, \tag{2}$$

$$[v_\alpha, v_\beta, v_x, v_y, v_{z1}, v_{z2}]^T = [C][v_{a1}, v_{b1}, v_{c1}, v_{a2}, v_{b2}, v_{c2}]^T,$$
$$[i_\alpha, i_\beta, i_x, i_y, i_{z1}, i_{z2}]^T = [C][i_{a1}, i_{b1}, i_{c1}, i_{a2}, i_{b2}, i_{c2}]^T.$$

With this transformation, the phase electrical variables are mapped onto the three mentioned subspaces and have clear physical meanings. In the principal plane, $\alpha - \beta$ currents are exclusively related to the flux/torque generation, whereas x-y currents only produce stator copper losses in IMs with distributed stator windings and negligible spatial harmonics. Moreover, in this case, zero-sequence currents cannot flow because the neutral points are isolated.

Figure 2 shows the 64 available switching states mapped onto the $\alpha - \beta$ and x-y subspaces. These voltage vectors are typically termed using the decimal number corresponding with their binary codification of the switching vector $[S]$. Focusing on Figure 2, it is observed that these available voltage vectors may be grouped into four concentric dodecagons according to their magnitude in the principal plane, termed large (C_L), medium-large (C_{ML}), medium (C_M) and small (C_S) vectors. On the other hand, there are four switching states with a null production in both subspaces.

Furthermore, using the rotating $d - q$ reference frame permits decoupling flux/torque to facilitate the regulation. Therefore, the torque production solely concerns the q-component, whereas the flux is related to the d-component. The rotation matrix that makes this decoupling possible is the Park transformation (3):

$$\left[D\right] = \begin{bmatrix} \cos\theta & sin\theta \\ -sin\theta & cos\theta \end{bmatrix}, \tag{3}$$

where θ is the rotor flux angle and is obtained via measured speed and estimated slip [25].

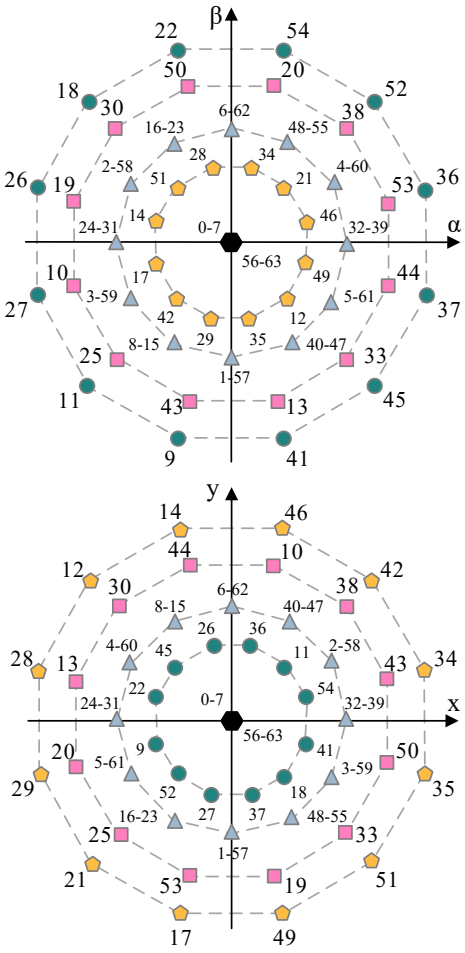


Figure 2. Available voltage vectors mapped onto $\alpha - \beta$ and x-y subspaces for the used 6PH-IM.

3. Multi-Vector MPC-Based Schemes Assessed

3.1. FCS-MPC

The most extended control structure of MPC-based strategies for multiphase electric drives is the FCS-MPC (Figure 3). This scheme does not require the employment of explicit modulation techniques as in other high-performance control strategies. The available control actions are evaluated by the algorithm to subsequently select the one that better achieves the control goals. In this manner, this regulation solution provides the switching states to be applied and, for this reason, it is termed as a direct control scheme.

As shown in Figure 3, the proportional–integral (PI) controller permits obtaining the q-current reference from the speed command. On the other hand, the d-current reference is set to its rated value to ensure a performance with nominal stator flux. In the inner-control loop, a discrete IM predictive model is employed, in this case, to adequately regulate the currents [23–27,31]. This work is based on VSD decomposition [51] to develop the IM model using a state-space representation. In this manner, the predictive model can be described using the expression (4):

$$\frac{d}{dt}\left[X_{\alpha\beta xy}\right] = [A] \cdot \left[X_{\alpha\beta xy}\right] + [B] \cdot \left[U_{\alpha\beta xy}\right], \tag{4}$$

where

$$\left[U_{\alpha\beta xy}\right] = \left[\bar{v}_{\alpha s}\,, \bar{v}_{\beta s}, \bar{v}_{xs}, \bar{v}_{ys},\ 0,\ 0\right]^T,$$

$$[X_{\alpha\beta xy}] = [i_{\alpha s},\ i_{\beta s},\ i_{xs},\ i_{ys},\ i_{\alpha r},\ i_{\beta r}]^T. \tag{5}$$

$[A]$ and $[B]$ are matrices that allow for characterizing the dynamics of the described 6PH-IM and are defined in detail in Appendix A. All the coefficients included in these matrices are dependent on the machine electrical parameters [52].

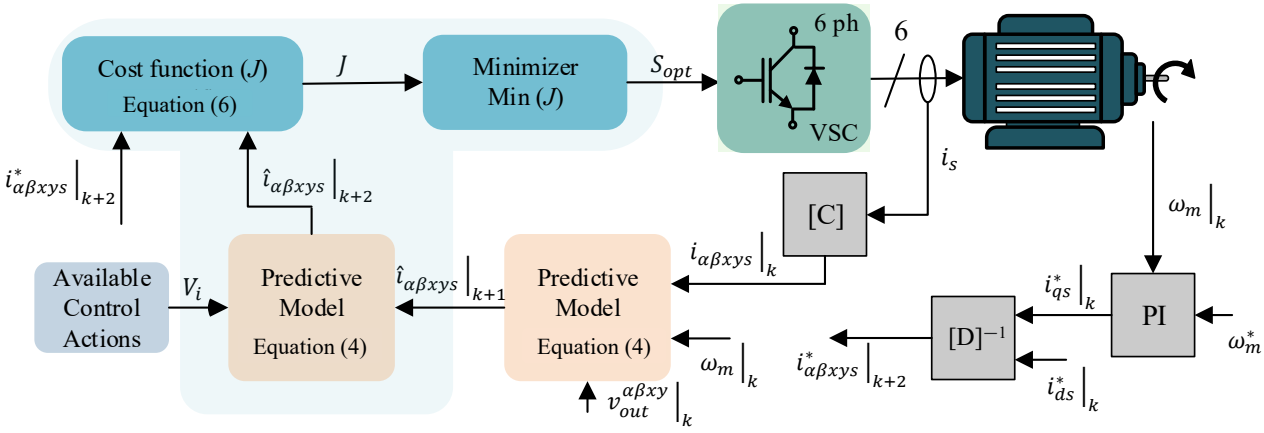


Figure 3. FCS-MPC scheme.

After the $k+1$ prediction stage, to avoid the one-step delay [53], a second prediction step $(k+2)$ permits estimating the future currents generated for each available switching state within the sampling period. All these predicted currents are evaluated using a cost function that includes the control objectives. A popular cost function for multiphase electric drive [52] is the one introduced in (6):

$$J = e^2_{\alpha s} + e^2_{\beta s} + K_{xy} \cdot (e^2_{xs} + e^2_{ys}), \tag{6}$$

with

$$\begin{aligned} e_{\alpha s} &= i^*_{\alpha s}|_{k+2} - \hat{i}_{\alpha s}|_{k+2}, \\ e_{\beta s} &= i^*_{\beta s}|_{k+2} - \hat{i}_{\beta s}|_{k+2}, \\ e_{xs} &= i^*_{x}|_{k+2} - \hat{i}_{x}|_{k+2}, \\ e_{ys} &= i^*_{y}|_{k+2} - \hat{i}_{y}|_{k+2}. \end{aligned} \tag{7}$$

The weighting factor K_{xy} is adequately adjusted to achieve the operating point required with minimum x-y current injection since these components provide a null torque/flux production in the considered electric drive. In this manner, the optimal control action is indicated by the minimum value derived from the cost function evaluation. This selected switching state is applied by the VSC in order to achieve these control objectives.

The selection of a single switching state using the cost function (6) promotes the relevance of the control objectives in main and secondary subspaces. However, the application of a single voltage vector makes it impossible to satisfy the voltage output requirements in both planes. This fact can generate an undesired harmonic injection in the x-y plane when the regulation goal is achieved in the main plane, resulting in a low current quality and an inadequate control performance. To address these problems, inherent to the performance of standard FCS-MPC, different multi-vector approaches have been proposed [23–33]. Four of them are evaluated in this work as previously exposed in Table 1.

3.2. VV-MPC

Standard FCS-MPC shows the mentioned problems related to the inherent harmonic injection in the secondary plane when the algorithm applies a single voltage vector per

sampling period. Fortunately, this limitation can be mitigated with the combination of several switching states during the sampling period. For that purpose, an initial step is the analysis of the control action location in the available subspaces. For instance, in the case of 6PH-IM, medium-large and large voltage vectors have the same direction in the fundamental plane and opposite direction in the *x*-*y* subspace (Figure 2). Taking advantage of this fact, VV-MPC [26] introduced, in the multiphase MPC area, the virtual voltage vector (VV) composition. This virtual voltage vector solution is designed offline with the aim of nullifying on average the *x*-*y* voltage generation. Two voltage vectors, large and medium-large, are applied at different times, t_l and t_{m-l}, respectively, during the sampling period to obtain zero average voltage output in the *x*-*y* plane. In this manner, the secondary subspace is regulated in open-loop mode. The general expression used to compose a VV is as follows:

$$VV_i = t_l \cdot V_l + t_{m-l} \cdot V_{m-l}, \tag{8}$$

$t_l = 0.73 \cdot T_m$ and $t_{m-l} = 0.27 \cdot T_m$, where T_m is the sampling period. Following this approach and taking into account the number of available large voltage vectors, 12 active VVs can be generated for the considered 6PH-IM (Figure 4).

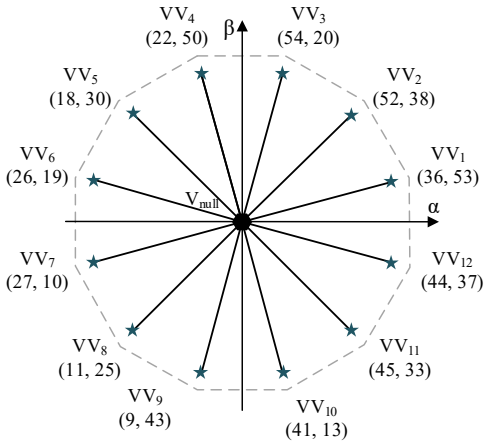


Figure 4. Available control actions in VV-MPC scheme.

The employment of these VVs also permits reducing the predictive model (9) and the cost function (11) (Figure 5), simplifying the control scheme and reducing the computational burden in relation to the standard version. Since the secondary currents can be regulated in open-loop mode with the null-average voltage production provided by the VVs in the secondary subspace, the following machine model and cost function can be employed:

$$\frac{d}{dt}\left[X_{\alpha\beta}\right] = [A] \cdot \left[X_{\alpha\beta}\right] + [B] \cdot \left[U_{\alpha\beta}\right], \tag{9}$$

where

$$\left[U_{\alpha\beta}\right] = \left[v_{\alpha s}\, v_{\beta s},\, 0,\, 0,\right]^T,$$

$$\left[X_{\alpha\beta}\right] = \left[i_{\alpha s},\, i_{\beta s},\, i_{\alpha r},\, i_{\beta r}\right]^T, \tag{10}$$

$$J = e_{\alpha s}^2 + e_{\beta s}^2. \tag{11}$$

This first multi-vector solution allowed for obtaining a significant improvement in terms of current quality over conventional FCS-MPC thanks to the simultaneous satisfaction of current requirements of both subspaces. In addition, its implementation provided a natural fault tolerance under open-phase faults with a reduced computational burden [54].

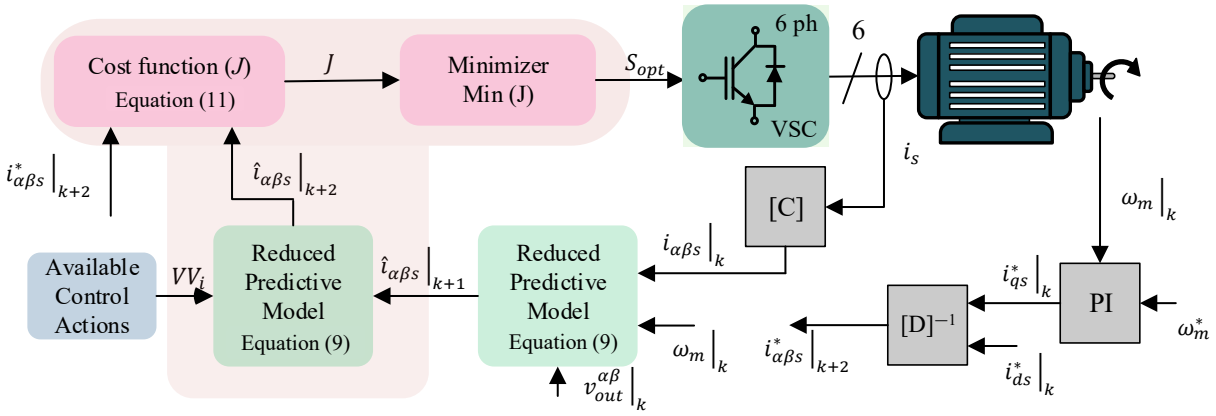


Figure 5. VV-MPC scheme.

3.3. LVV-MPC

Although the introduction of the described VVs resulted in a notable enhancement over the standard FCS-MPC [26], this solution presented certain limitations. The inclusion of medium-large voltage vectors to compose a multi-vector response leads to a limitation in the dc-link voltage usage. The voltage output reduction in relation to a large vector (LV) is 7.2% and this fact entails a decrease in the operating range. On the other hand, a second shortcoming is observed in the VV-MPC scheme. Even though VV control actions provide an average cancellation of voltage output in the secondary plane, the application of a medium-large voltage vector during 27% of the T_m generates high instantaneous voltage values in the secondary subspace. This voltage behavior can result in the injection of high current harmonics in this x-y subspace when the stator impedance presents low values.

LVV-MPC addresses these limitations, introducing a set of virtual voltage vectors that avoids the employment of medium-large voltage vectors to compose virtual voltage outputs [25]. The proposed control actions are formed exclusively by two adjacent large voltage vectors and hence they are termed LVVs (Figure 6). These couples of two large voltage vectors permit a 96.6% dc-link usage (Table 2), thus augmenting the operation range over VV-MPC. Moreover, the use of solely large voltage vectors that are mapped onto the secondary plane as small vectors results in low instantaneous x-y voltages. In this case, it is not possible to provide a zero average x-y voltage output since the small vectors corresponding to adjacent large vectors are shifted 150°, but it can be notably reduced. These reduced x-y voltage values derived from the use of LVVs also permit controlling the secondary subspaces in open-loop mode. Furthermore, it is possible to employ a reduced machine model and cost function as well as in [26] (Figure 7). It is also noteworthy that the LVV control actions present a lower switching frequency than VVs since the number of switching changes between adjacent large voltage vectors is only one, whereas, between large and medium-large vectors, it is two. As well as in VV-MPC, the available control actions in LVV-MPC are 12 active virtual voltage vectors and a null vector. The general expression used to compose a control action in LVV-MPC is as follows:

$$LVV_i = t \cdot LV_j + t \cdot LV_k, \tag{12}$$

where $t = 0.5 \cdot T_m$. The subscripts j and k refer to adjacent large vectors.

Table 2. Dc-link usage in the evaluated MPC schemes.

VV-MPC	LVV-MPC	PULLA-MPC	MV5-MPC
92.8 %	96.2 %	96.2 %	89.9 %

The results obtained with this solution of control actions promoted a new trend from the perspective of the composition of virtual voltage vectors.

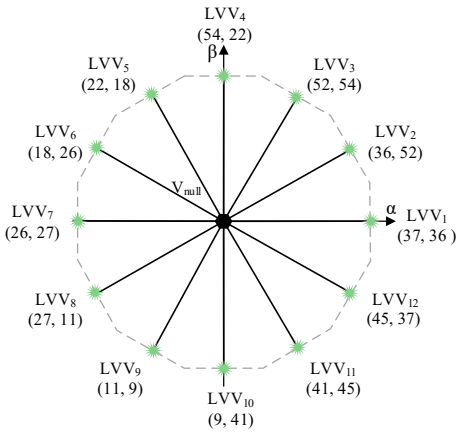


Figure 6. Available control actions in LVV-MPC scheme.

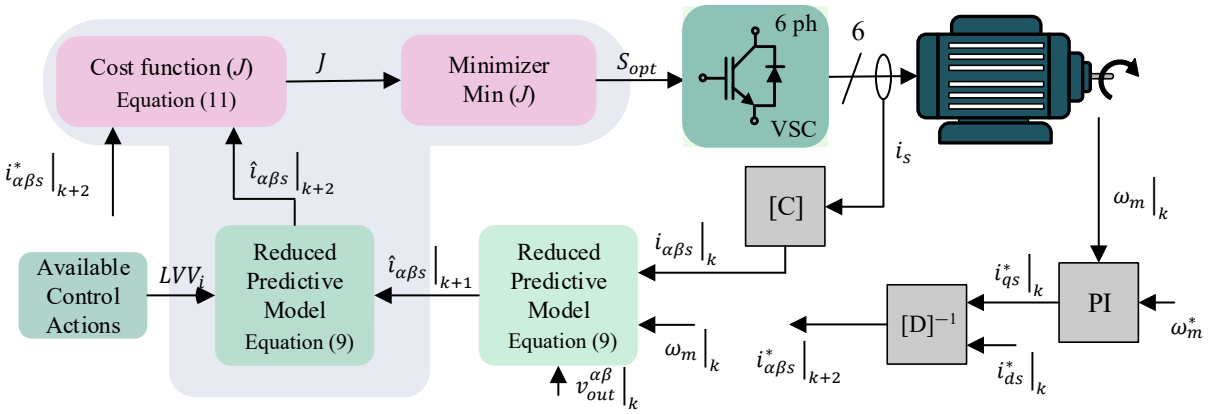


Figure 7. LVV-MPC scheme.

3.4. PULLA-MPC

LVV-MPC allowed for improving some VV-MPC shortcomings. However, both schemes presented a deteriorated performance in low-speed regions due to the static nature of the control actions. In spite of the significant reduction in x-y current injection, the low voltage output refinement provided in the $\alpha - \beta$ subspace does not allow for an adequate adjustment to the operating point. Moreover, the usage of active control actions cannot be regulated according to the operating conditions during the sampling period. In contrast, the offline determination of the VV and LVV control actions entails a reduced computational burden.

Certain solutions addressed the improvement of the voltage output refinement using an online calculation of the control actions [55], leading to a higher computational burden. PULLA-MPC [24] introduces a multi-vector set of online calculated control actions that provides an enhanced voltage refinement in the main subspace. In addition, the injection of secondary currents can be modified, taking into account the specific operating conditions. In this case, the active control actions of PULLA-MPC are composed of the LVVs [24] combined with a zero vector (Figure 8). In this manner, it is possible to generate low current injection in the secondary plane and, thanks to the use of the null voltage vector, improve the adjustment to the operating point. The proper null vector for each LVV is selected in order to generate minimum switching changes, reducing the switching frequency (f_{sw}).

The use of an analytic function based on the operating conditions for the calculation of the application times leads to a reduced computational cost in relation to other previous works that perform iterative processes. In the case of PULLA-MPC, the application time was estimated as follows:

$$t_{apl} = k_{apl} \cdot \frac{i_{qs}^{*}|_k}{i_{qs}|_{max}} \cdot T_m, \tag{13}$$

where

$$k_{apl} = 0.901 + 0.022 \cdot i_{qs}^{*}|_k. \tag{14}$$

Thus, the general expression (15) used to determine the average voltage output in the PULLA control actions is as follows:

$$PVV_i = t_{apl} \cdot (0.5 \cdot LV_j + 0.5 \cdot LV_k) + (1 - t_{apl}) \cdot V_{null}. \tag{15}$$

These control actions also allowed for regulating x-y currents in open-loop mode and decreasing the computational burden thanks to the usage of a reduced predictive model (9) and cost function (11). Figure 9 shows the PULLA-MPC regulation scheme.

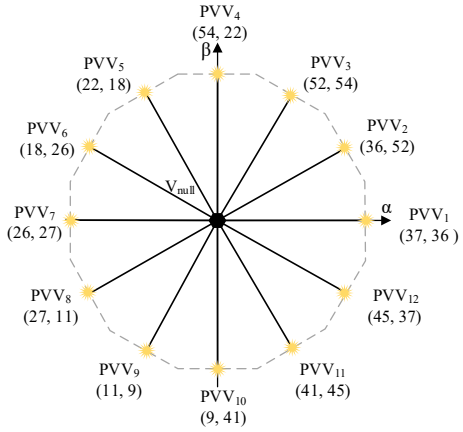


Figure 8. Available control actions in PULLA-MPC scheme.

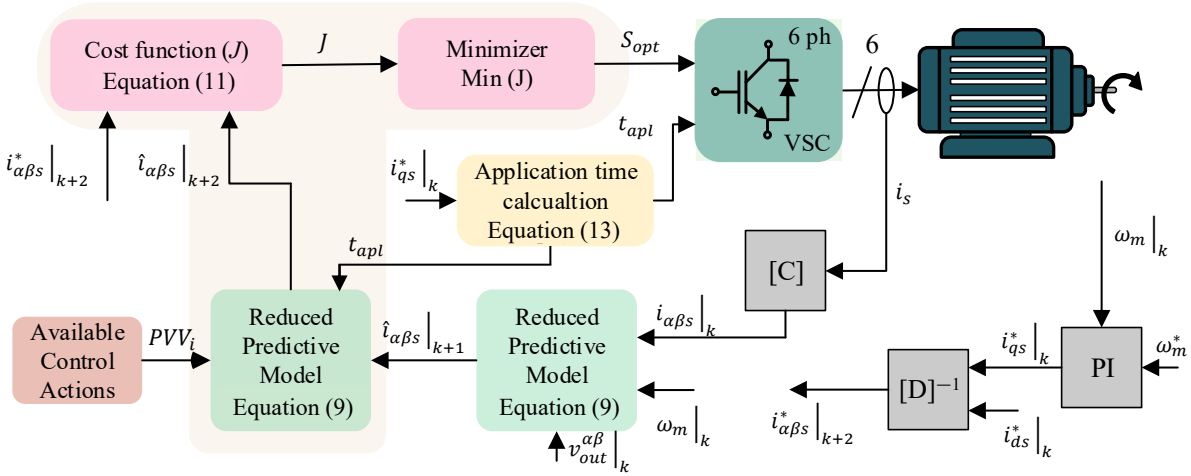


Figure 9. PULLA-MPC scheme.

3.5. MV5-MPC

In spite of the improvements introduced with the PULLA-MPC (a better voltage refinement for achieving the flux/torque requirement, a reduced harmonic injection and a decreased computational cost), the x-y current mitigation could still be enhanced. Searching for a further improvement in terms of current quality, the MV5-MPC [27] strategy focuses on the mitigation of the remaining current harmonics. Despite the application of PULLA control actions permitting achieving a notable reduction in the x-y, the full

mitigation of the average *x*-*y* voltage output cannot be obtained when this control solution is implemented.

MV5-MPC introduced a set of enhanced control actions characterized by a null average *x*-*y* voltage output with low instantaneous values. As explained in [23], the application of a minimum of three adjacent large voltage vectors allows for nullifying the average voltage output in the secondary plane. Moreover, the use of zero switching states reduces the harmonic distortion by enabling a radial adjustment to the operating scenario. In the MV5-MPC case, the control actions are formed by the application of four adjacent large voltage vectors and a selected null vector (Figure 10), going further than [23] in the current quality improvement and the associated stator copper losses. As mentioned, the composition of these control actions includes an adequate choice of the null switching state in order to minimize the resultant switching frequency.

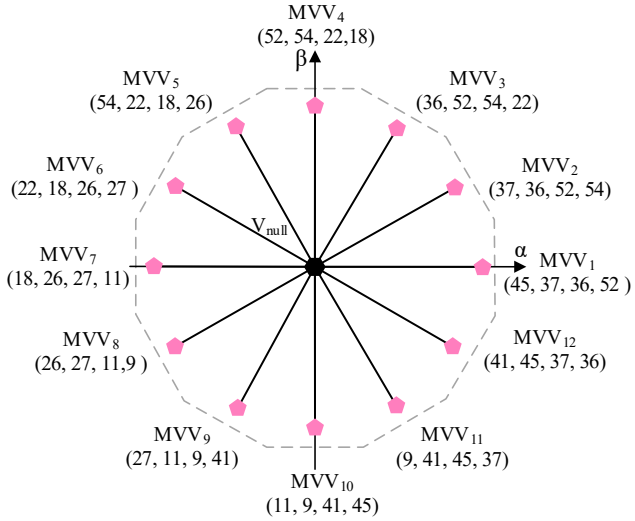


Figure 10. Available control actions in MV5-MPC scheme.

The application time t_{apl} of the four active vectors is determined according to the operating scenario (16) and thus limits the production of *x*-*y* voltages. The complementary time will be applied to the null voltage vector within the sampling period.

$$t_{apl} = \frac{i^*_{qs}|_k}{i_{qs}|_{max}}. \tag{16}$$

The set of control actions in MV5-MPC is also formed by 12 active virtual voltage vectors and a null voltage vector. The voltage output provided for each control action can be determined as follows:

$$\begin{bmatrix} v^{\alpha}_{out} \\ v^{\beta}_{out} \\ v^{x}_{out} \\ v^{y}_{out} \end{bmatrix} = \begin{bmatrix} V^{\alpha}_{l1} & V^{\alpha}_{l2} & V^{\alpha}_{l3} & V^{\alpha}_{l4} & V^{\alpha}_{null} \\ V^{\beta}_{l1} & V^{\beta}_{l2} & V^{\beta}_{l3} & V^{\beta}_{l4} & V^{\beta}_{null} \\ V^{x}_{l1} & V^{x}_{l2} & V^{x}_{l3} & V^{x}_{l4} & V^{x}_{null} \\ V^{y}_{l1} & V^{y}_{l2} & V^{y}_{l3} & V^{y}_{l4} & V^{y}_{null} \end{bmatrix} \begin{bmatrix} t_{apl} \cdot t_1 \\ t_{apl} \cdot t_2 \\ t_{apl} \cdot t_3 \\ t_{apl} \cdot t_4 \\ 1 - t_{apl} \end{bmatrix}, \tag{17}$$

where, for any group of adjacent large vectors (i.e., V_{36}, V_{52}, V_{54} and V_{22}), an adequate balance is obtained with the following per-unit duty cycles: $t_1 = 0.1 \cdot T_m$, $t_2 = 0.3412 \cdot T_m$, $t_3 = 0.3909 \cdot T_m$ and $t_4 = 0.1679 \cdot T_m$, respectively.

In (18), the general expression for an MV5-MPC control action strategy is shown.

$$MVV_i = t_{apl} \cdot (t_1 \cdot LV_j + t_2 \cdot LV_k + t_3 \cdot LV_m + t_4 \cdot LV_n) + (1 - t_{apl}) \cdot V_{null}, \tag{18}$$

where j, k, m and n refer to adjacent large voltage vectors. The application of these control actions has allowed for obtaining similar current quality results to other regulation schemes with an explicit modulation stage (IRFOC with carrier-based PWM) [27] for a lower switching frequency. In addition, MV5-MPC schemes, thanks to the design of their control actions, also permit regulating these x-y currents in open-loop mode. Consequently, it is possible to employ a reduced predictive machine model (9) and a simple cost function (11). Figure 11 shows the scheme of the described MV5-MPC.

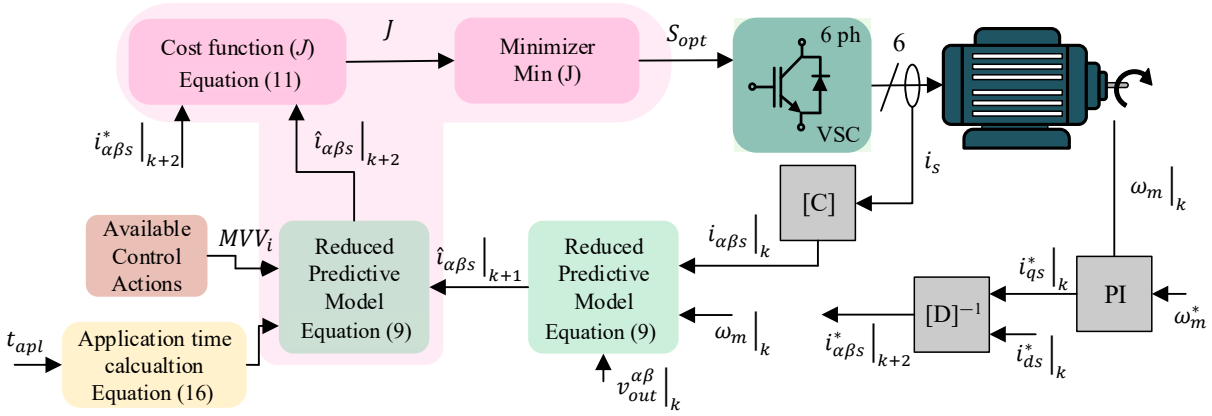


Figure 11. MV5-MPC scheme.

4. Influencing Factors Used to Select an Adequate Multi-Vector MPC Scheme

This section aims to provide some insight into the influencing factors that a control designer should consider when selecting the proper multi-vector MPC scheme. With this goal in mind, this first stage is the definition of the ideal characteristics of a control strategy in steady-state scenarios:

1. High current quality.
2. Suitable current tracking.
3. Minimal power losses.

In the multiphase case, there are numerous factors that may affect each of these desired control requirements. Some of the most significant influencing factors in the case of MPC for multiphase electric drives are:

IF1. Spatial and time harmonics [13,56].
IF2. Secondary components [18,57].
IF3. Electric parameter values [42,58].
IF4. Usage of the available dc-link voltage [59,60].
IF5. Control action nature [23,27].

4.1. Current Quality in Multiphase Electric Drives

As above-mentioned, this work employs electric drives that include IMs with two sets of three-phase windings. The study of the harmonic content, noted as IF1, using this arrangement is a fundamental part in the regulation scheme selection. In six-phase electric drives, different harmonic components are mapped onto the three orthogonal planes after the VSD transformation depending on the stator winding shifting [61], being in this case an asymmetrical arrangement (30°). Spatial harmonics, motivated by the reluctance variation in the airgap and the employment of concentrated windings, are considered negligible in this work since the IM presents a stator with distributed windings. This winding arrangement entails a sinusoidal MMF in the airgap; thus, these harmonic components shall be neglected. Regarding the time harmonics, they are mapped onto the three available planes in the case of 6PH-IM. The $\alpha - \beta$ subspace holds the 11th and 13th as the first low-order harmonics. Conversely, the 5th and 7th harmonics are the first low-order harmonics mapped onto the secondary plane, whereas the 0_+0_- subspace is concerned with the DC

component and triplen harmonics (3rd, 9th, 15th, ...) but, in this winding configuration, they do not flow because the two neutral points are isolated. In addition, the possible asymmetries in the machine, the impact of the applied switching states or the deadtime in the semiconductor lead to a deterioration in the current quality.

As mentioned, the switching pattern applied in the sampling period presents a paramount effect on the harmonic content of the current signal. In the considered 6PH-IM with distributed windings, the switching states with an active production in the principal plane also generate a voltage output in the secondary. Consequently, this results in the injection of unwanted current harmonics. For this reason, the designer must evaluate the influence of IF2 on the waveform quality and on the rest of the intended electric drive features. Such injected currents are the response to the application of the *x*-*y* voltage output in an *RL* circuit where the leakage stator inductance is L_{ls} and the stator resistance R_s, as has been described in [57]. Figure 12 shows the evolution of the *x*-*y* currents resulting from the application of one active control action of the considered multi-vector MPC strategies. Furthermore, Figure 12 presents the *x*-*y* currents obtained with low and high stator impedance values since the impact of IF3 should be considered. The theoretical study included in Figure 12 about the *x*-*y* currents warns about its influence. Focusing on the left column of Figure 12a (VV-MPC scheme), the so-called *average deception* is clearly observed [27]. Two active voltage vectors, large and medium-large, are applied in the same sampling period to cancel on average the *x*-*y* voltage generation. However, the peak values are not taken into account, resulting in high values of peak-to-peak (PtP) *x*-*y* current values and worsening the current quality. MV5-MPC also permits nullifying the *x*-*y* voltage generation in a sampling period. Nevertheless, in this case, the application of four active large voltage vectors and the null vector allows for reducing the PtP current values (Figure 12d). It is noteworthy that, due to the increase in the stator inductance, the differences among the selected multi-vector approaches can practically be neglected from the point of view of the secondary components. In this work, all the assessed multi-vector control schemes are performed using the same sampling period. Thus, a higher current quality is expected in those regulation schemes that apply a higher number of switching states in the sampling period.

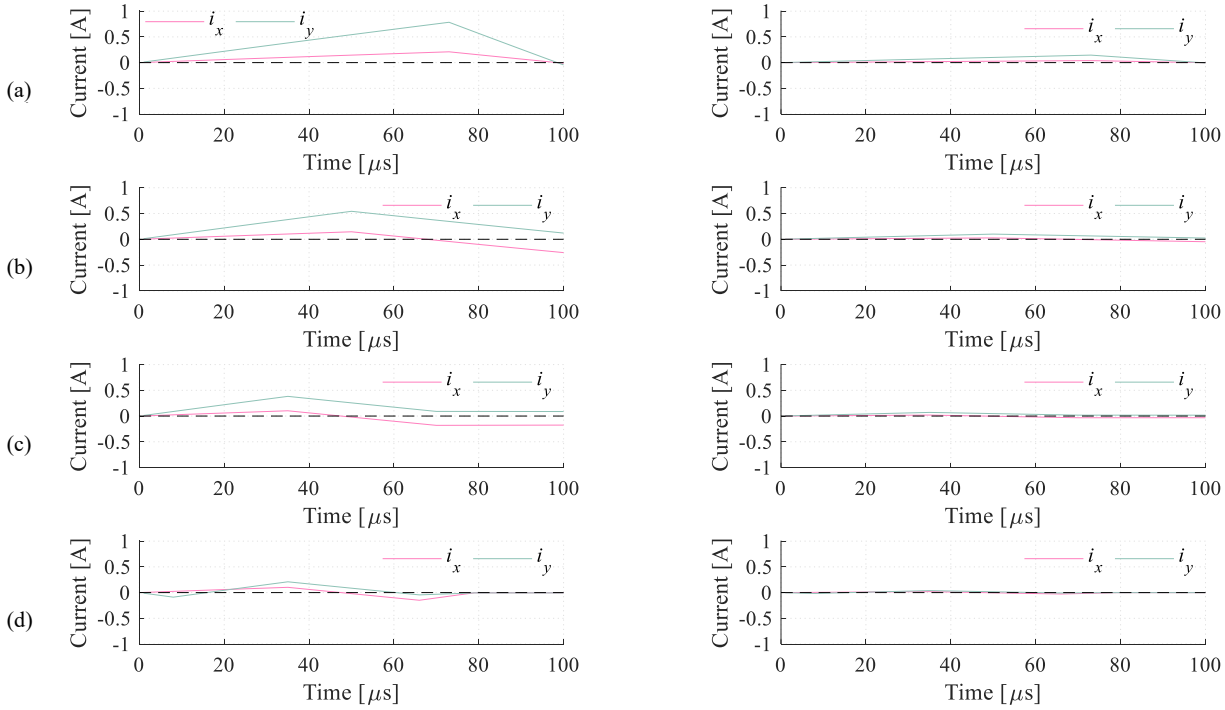


Figure 12. Theoretical analysis of *x*-*y* currents for the different control actions applied in the evaluated multi-vector MPC strategies. (**a**) VV-MPC, (**b**) LVV-MPC, (**c**) PULLA-MPC and (**d**) MV5-MPC. Left column is 6PH-IM1 (low stator impedance) and right column is 6PH-IM4 (high stator impedance).

4.2. Current Tracking Performance

To characterize the current quality, the THD and PtP values of the x-y currents have been used in this electric drive evaluation. In the same manner, to evaluate the effectiveness of the current tracking in steady state, the mean square error (MSE) of the main components is employed. The MSE of the d-current and q-current describes the adequacy of these currents to their references, related to flux and torque production, respectively. In this regard, the influence of IF4 and IF5 in the regulation performance should be analyzed.

A satisfactory voltage output adjustment requires the availability of control actions that permit satisfying flux and torque requirements. A higher refinement in the voltage output leads, in turn, to a better current tracking and thus to a suitable control performance. Since discrete and adaptive control actions are available in the assessed schemes, the designer should evaluate IF5 to select the adequate regulation scheme. Since, in the considered multi-vector approach, the duty cycles can be estimated using offline and online alternatives, the obtained refinement is notably different. On the other hand, the possibility of applying two, three of four switching states to form the active control action presents a certain influence in the usage of dc-link voltage as shown in Table 2. The higher the number of switching states applied in a sampling period, the lower the dc-link voltage availability. Therefore, as shown in Table 2, MV5-MPC presents the lowest dc-link utilization among the assessed multi-vector MPC schemes. For this reason, the influence of IF4 should also be considered when selecting the proper multi-vector control scheme.

On the other hand, the required voltage outputs can be provided using discrete control actions (VV-MPC and LVV-MPC schemes) or an adaptive response, as in the case of PULLA-MPC or MV5-MPC. The calculation of the application times for this adaptive voltage output must be accurate to adequately adjust to the reference. Thus, it can be obtained using (13).

It should be highlighted that (19) is an enhanced expression that permits a more suitable application time (t_a) calculation, since all active currents are considered in the estimation process:

$$t_a = \frac{i^*_{qs}|_k + i^*_{ds}|_k}{i_{qs}|_{max} + i_{ds}|_{max}}, \tag{19}$$

However, both works [24,27] only consider the q-current to obtain the application time. For this reason, (13) is employed in the developed analysis.

It can be expected that the implementation of a multi-vector scheme that employs discrete control actions may lead to higher d- and q-current tracking errors at low operating points. The selection of multi-vector approaches with adaptive control actions permits addressing this problem, using the inclusion of the null voltage vector as an applied switching state. However, the dc-link usage may result in a deterioration in the control performance, as shown in Section 5.

4.3. Minimal Power Losses

Beyond a suitable control performance, an electric drive should reach its regulation objectives with reduced associated losses. Therefore, it is convenient to evaluate the global losses, i.e., power losses in the VSC and in the 6PH-IM. Focusing on the influencing factors in VSC power losses, they are related to the switching rate and the RMS phase current values [62]. Regarding the switching losses of the VSC, they can be estimated as shown in (20):

$$P_{sw} = 12 \cdot (P_{sw_{on}} + P_{sw_{off}} + P_{sw_{rr}}), \tag{20}$$

where

$$\begin{aligned} P_{sw_{on}} &= E_{on} \cdot f_{sw}, \\ P_{sw_{off}} &= E_{off} \cdot f_{sw}, \\ P_{sw_{rr}} &= E_{rr} \cdot f_{sw}. \end{aligned} \tag{21}$$

The terms E_{on}, E_{off} and E_{rr} are the turn on, turn off and reverse recovery energy losses, respectively, and $P_{sw_{on}}$, $P_{sw_{off}}$ and $P_{sw_{rr}}$ are the associated power losses. The determination of these energy values (E_{on}, E_{off} and E_{rr}) can be obtained using the expressions included in (22), where the reference values are collected from the IGBT datasheets. The exponent K_i takes the value 1 if energetic analysis is performed on the IGBT or 0.55 if the free-wheeling diode (FWD) is studied. E_{ref} and I_{ref} values are also obtained from the technical data provided by the corresponding manufacturer.

$$\begin{aligned} E_{on} &= E_{ref_{on}} \cdot \left(\frac{RMS}{I_{ref}}\right)^{K_i}, \\ E_{off} &= E_{ref_{off}} \cdot \left(\frac{RMS}{I_{ref}}\right)^{K_i}, \\ E_{rr} &= E_{ref_{rr}} \cdot \left(\frac{RMS}{I_{ref}}\right)^{K_i}. \end{aligned} \tag{22}$$

Therefore, the switching losses increase when the switching frequency and RMS current are higher. Since, for a fixed operating point, the RMS current is equal for the selected control schemes, the switching frequency can be considered as the main influencing factor in this regard. At this point, it should be noted that applying adjacent large voltage vectors reduces the switching frequency because only one switching variation appears. This is the case in LVV-MPC, PULLA-MPC and MV5-MPC schemes. The VV-MPC strategy applies control actions composed of a large voltage vector and a medium-large one, resulting in two switching changes per control action. On the other hand, the implementation of a variable application time approach based on the usage of the null voltage vector also increases the switching frequency because a higher number of switching changes appear. Thus, the impact of IF5 in relation to the desired features of the electric drive operation should be considered.

To evaluate the total electrical losses involved in the assessed multiphase electric drives, the conduction losses of VSC semiconductors must also be determined. The expressions (23) and (24) [62] are employed to calculate the latter.

$$P_{con,X} = R_X \cdot I_X^2 + V_X \cdot i_{X_{ave}}, \tag{23}$$

where

$$\begin{aligned} R_X &= \left(\frac{R_2 \cdot T_{min} - R_1 \cdot T_{max}}{\Delta T}\right) + \left(\frac{R_1 - R_2}{\Delta T} \cdot T_j\right), \\ V_X &= \left(\frac{V_2 \cdot T_{min} - V_1 \cdot T_{max}}{\Delta T}\right) + \left(\frac{V_1 - V_2}{\Delta T} \cdot T_j\right), \\ \Delta T &= T_{min} - T_{max}. \end{aligned} \tag{24}$$

The values T_{min} and T_{max} are included in the device datasheet. On the other hand, the values R_1 and V_1, related to T_{min}, are obtained from the datasheet graphs. In the same way, R_2 and V_2, related to T_{max}, are determined, observing the graphical information attached to the datasheet. The subindices X refer to the device parts, IGBT or FWD. The term I_X refers to RMS values and $i_{X_{ave}}$ to mean current values. Thus, the total conduction power losses can be estimated using (25).

$$P_{con} = 6 \cdot (P_{con_{IGBT}} + P_{con_{FWD}}). \tag{25}$$

These conduction losses are strongly related to the RMS phase current values and are the most influencing factor in the production of these types of losses. In addition, a dependence on the operating point appears since the higher the performance region is, the higher the RMS values are.

Regarding the other losses in the electric drive, the stator copper losses can also be considered as a main influencing factor in the electric drive performance in terms of power losses. These losses are related to the conduction, in this case, through IF3, concretely, the stator impedance. Therefore, these losses increase by the RMS value of the phase currents and carry it out in quadratic relation as in (26). Consequently, as occurs in VSC conduction losses, the stator copper losses also show an operating point dependence.

$$P_{stator} = 6 \cdot R_s \cdot I_{RMS}^2. \quad (26)$$

Thus, in those 6PH-IMs characterized by an augmented stator resistance (R_s), it is necessary to analyze its influence on the various abovementioned aspects rather than simply expecting a significant value of stator copper losses, especially in high speed and torque scenarios.

It is definitely necessary to consider multiple aspects for the proper selection of a multi-vector MPC scheme, such as switching frequency, harmonic injection, dc-link utilization, IM stator parameters and even the operating point of the electric drive to be controlled. In this work, the impact of these influencing factors is evaluated from three perspectives: the current quality, the current tracking performance and the power losses involved in the electric drive energy conversion. From these three points of view, the results obtained in the test bench are introduced and analyzed in the following section.

5. Experimental Validation

5.1. Experimental Setup

The experimental platform shown in Figure 13 has been employed to carry out the assessment of the considered multi-vector MPC schemes. This multiphase electric drive is formed by an asymmetrical six-phase IM with two sets of three-phase windings spatially shifted 30° fed by a dual three-phase two-level VSC (Semikron SKS22F). As previously exposed, the stator parameters need to be modified in order to obtain conclusions with a higher degree of generality. For that purpose, six sets of passive loads with resistor and inductive parts have been connected to the 6PH-IM stator. Specifically, four different IM machines with remarkably dissimilar stator parameters have been employed in this work (see Table 3). Among the selected electrical motors, 6PH-IM1 is the IM with the lowest impedance whereas 6PH-IM4 is the machine characterized by the highest stator impedance. 6PH-IM2 has a stator resistance (R_s) higher than 6PH-IM1 while the stator leakage inductance (L_{ls}) remains the same for both. 6PH-IM3 and 6PH-IM1 both maintain the same R_s value but the former shows an augmented value of L_{ls}. On the other hand, the shaft of the six-phase IM is coupled to a DC machine working as a generator. A variable resistor load is connected to the armature. Therefore, the load torque is speed-dependent in this electric drive. The selected control schemes are implemented in a digital signal processor from Texas Instruments, TI, (TMS320F28335) using a J-TAG connector and the TI property software (Code Composer Studio). Focusing on the sampling period, the same value has been employed for the considered control techniques (100 µs). Finally, the work provides the obtained experimental results as additional data. This Supplementary Material can be employed to reply to the results or to carry out additional analyses.

Table 3. 6PH-IM electrical parameters.

Dc-Link Voltage = 300 V; Control Frequency 10 kHz				
Parameter	**6PH-IM1**	**6PH-IM2**	**6PH-IM3**	**6PH-IM4**
$R_s(\Omega)$	4.2	14.2	4.2	14.2
$R_r(\Omega)$	3	3	3	3
L_m (mH)	370	370	370	370
L_{ls} (mH)	4.5	4.5	24.5	24.5
L_{lr} (mH)	55.12	55.12	55.12	55.12

(R_r: rotor resistance, L_m: mutual inductance, L_{lr}: rotor leakage inductance and L_{ls}: stator leakage inductance).

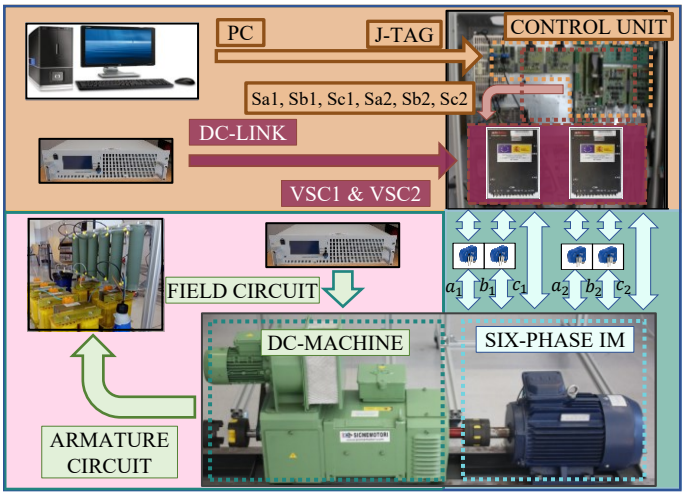


Figure 13. Experimental test bench.

5.2. Experimental Results

This section includes the experimental results, where the performance of the aforementioned VV-MPC [26], LVV-MPC [25], PULLA-MPC [24] and MV5-MPC [27] strategies has been tested. For that purpose, each regulation technique has been evaluated in different steady-state scenarios. The variation in the reference speed (250, 500 and 750 rpm) and the load resistance (33, 50 and 100 Ω) has allowed for the generation of diverse operating conditions. The proposed comparison employs different performance indices that assess the current quality, control performance, switching frequency and total losses in the electric drive.

5.2.1. Current Quality Analysis

There are multiple indices that permit assessing the current quality. In this work, the THD, the RMS of phase currents and the PtP values of the secondary currents have been selected to evaluate the goodness of the analyzed control schemes. Figure 14 shows the behavior of the mentioned algorithms according to the proposed quality indices: THD (Figure 14a), RMS (Figure 14b) and PtP (Figure 14c). It is well known that the implementation of a multi-vector MPC is a suitable solution in multiphase electric drives when a current quality enhancement is required [23–28,39].

Observing Figure 14a, the multi-vector solution MV5-MPC can be defined as the best choice from the THD perspective, regardless of the analyzed 6PH-IM. This enhancement in the current quality is achieved thanks to the use of a higher number of voltage vectors per control period, as well as the usage of a variable application time. The price to be paid for this lower harmonic distortion is a higher switching frequency, as shown in Figure 15. Focusing on the use of variable times of application, this concept overcomes the static nature of VV-MPC and LVV-MPC schemes. The impact of this term on the THD is easily observable in the comparison between PULLA-MPC and LVV-MPC since both strategies employ the same active control actions.

In spite of the mentioned improvement, it is important to highlight that the differences in terms of THD are strongly dependent on the stator parameters (IF3) and control action nature (IF5). In fact, in Figure 14a right column, it is observed that a similar harmonic distortion is obtained in the considered 6PH-IM4. This lower THD is derived from the filtering effect carried out by the augmented stator impedance. In this regard, Figure 16 illustrates the waveform of the phase currents for the implemented algorithms when the configurations 6PH-IM1 and 6PH-IM4 are employed. As shown in the right column of Figure 16, the variances between the studied MPC schemes are minimal when the test bench 6PH-IM4 is selected. These results have been obtained using the same control periods and, consequently, significant differences appear in terms of switching frequencies, as

shown in Figure 15. The mentioned variations in the THD are even lower when the control schemes are implemented using the same switching frequency. This fact can be observed in Figure 17, where the phase currents are again depicted for 6PH-IM1 and 6PH-IM4. To obtain a generalized comparison in terms of current quality, in Figures 16 and 17, the phase currents obtained using an IRFOC scheme based on a PWM stage have been depicted.

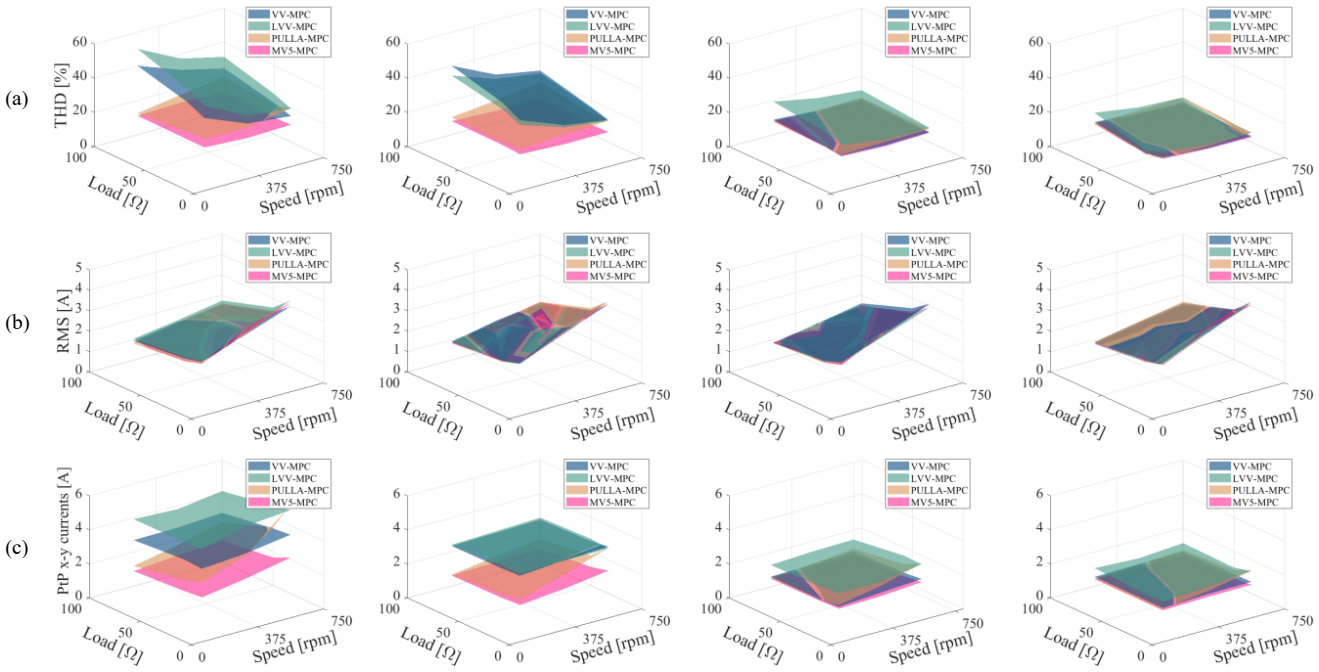


Figure 14. Selected indices for evaluating the current quality in the experimental tests. (**a**) THD phase current, (**b**) RMS phase current and (**c**) peak-to-peak x-y current. From left column to right: 6PH-IM1, 6PH-IM2, 6PH-IM3 and 6PH-IM4.

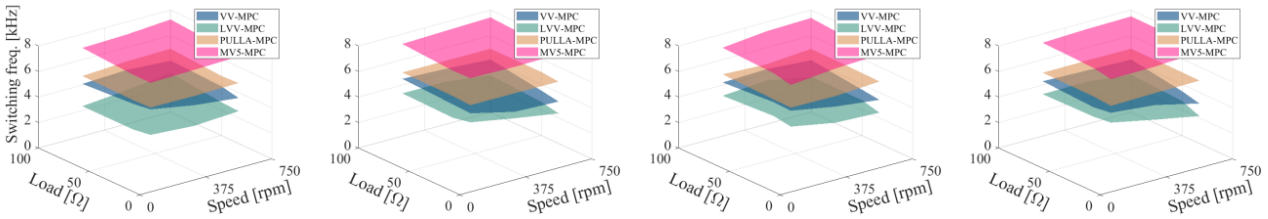


Figure 15. Switching frequency obtained in the experimental tests. From left column to right: 6PH-IM1, 6PH-IM2, 6PH-IM3 and 6PH-IM4.

As previously exposed in Section 3, the behavior of the secondary components is significantly dependent on the value of the stator impedance, as shown in Figure 14c. These experimental results confirm the theoretical analysis presented in the previous section (Figure 12). Focusing on the performance of the considered multi-vector solutions, MV5-MPC is the best option for mitigating the injection of the x-y currents regardless of the employed IM. The increase in the stator resistance produces a significant improvement in the case of LVV-MPC (see Figure 14c for 6PH-IM2) even though a lower switching frequency is employed.

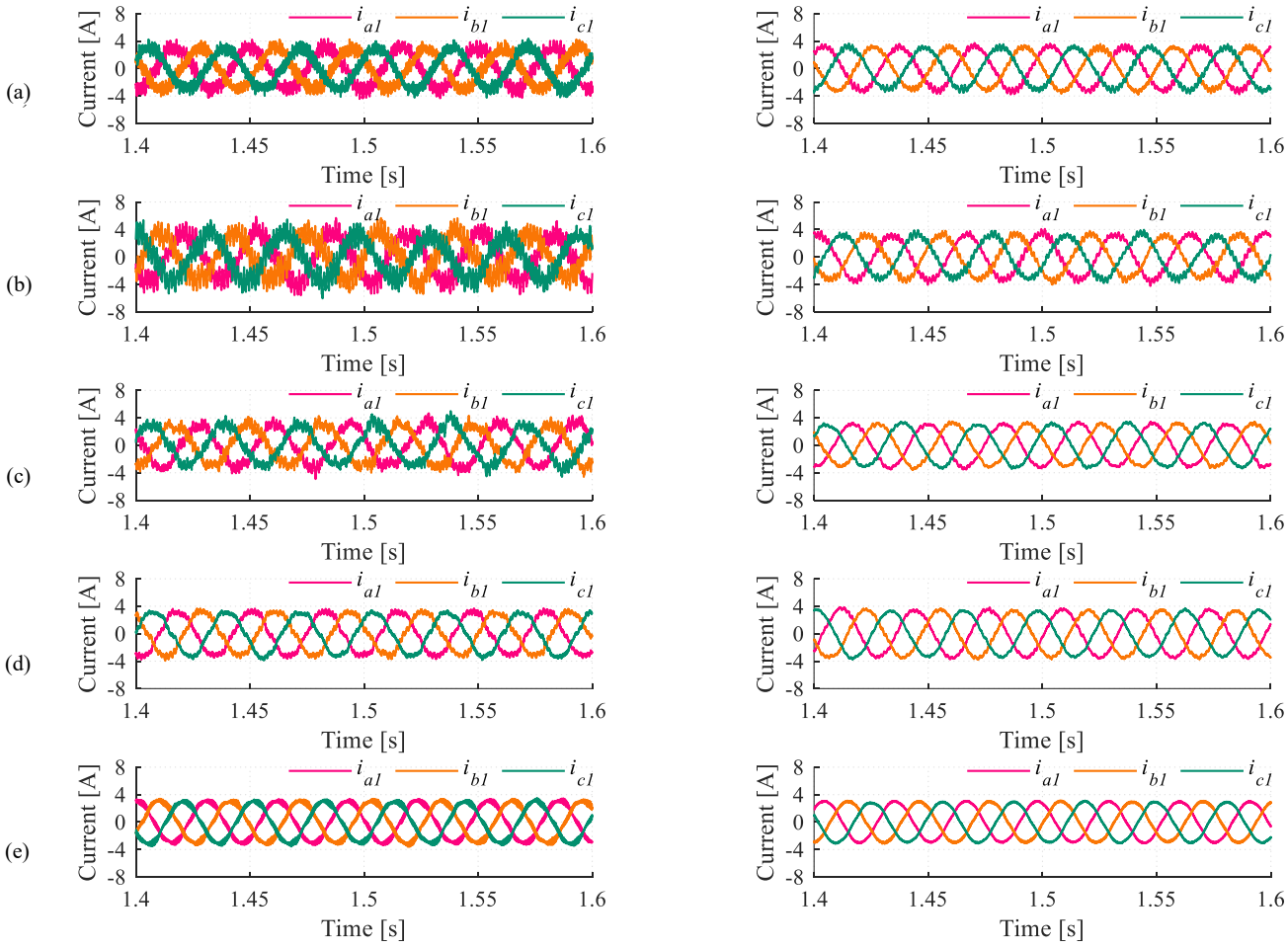


Figure 16. Phase currents at 500 rpm using different multi-vector control schemes implemented with the same sampling period. (**a**) VV-MPC, (**b**) LVV-MPC, (**c**) PULLA-MPC, (**d**) MV5-MPC and (**e**) IRFOC. From left to right columns: 6PH-IM1 and 6PH-IM4.

As shown in the right plot of Figure 14c, the increase in stator impedance makes the employment of variable times of application also negligible. For this reason, a similar PtP value of the secondary currents is obtained, although the available control actions are characterized by a static nature, as in the case of VV-MPC and LVV-MPC. Therefore, the selection of the control scheme can be conditioned to an important degree by the stator impedance value if additional control goals are crucial for the industrial application.

Focusing on the RMS value of the phase currents, non-significant differences can be observed regardless of the implemented control scheme or the employed electric drive (see Figure 14b).

5.2.2. Current Tracking Performance

This section assesses the abilities of the mentioned multi-vector MPC techniques to provide a suitable tracking of the reference currents. This issue is crucial for ensuring the suitable performance of the IM. With that in mind, the MSE of the $d-q$ currents has been selected as the basis for the comparison.

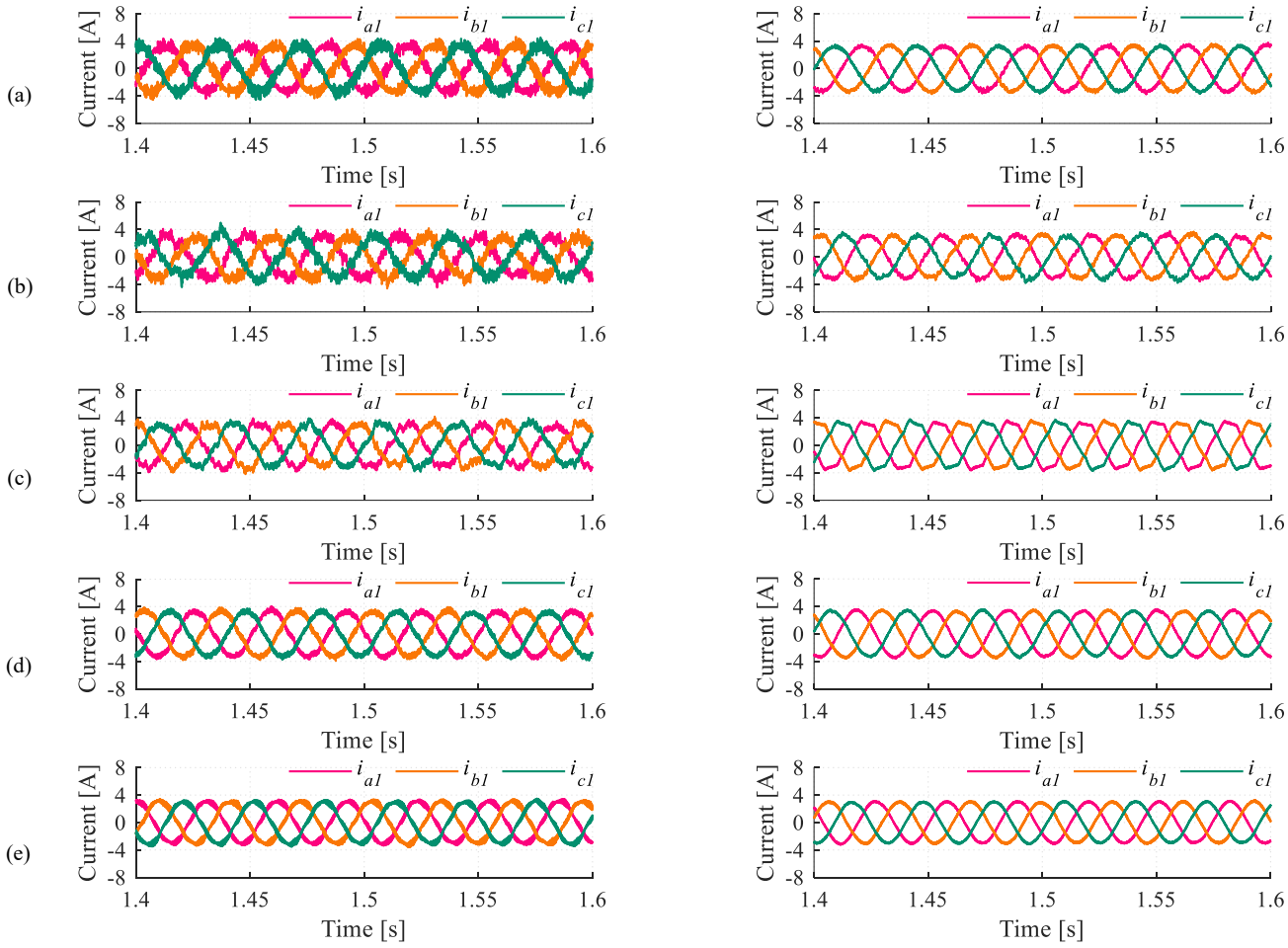


Figure 17. Phase currents at 500 rpm using different multi-vector control schemes implemented with the same switching frequency. (**a**) VV-MPC, (**b**) LVV-MPC, (**c**) PULLA-MPC, (**d**) MV5-MPC and (**e**) IRFOC. From left to right columns: 6PH-IM1 and 6PH-IM4.

In the case of 6PH-IM1, characterized by a low stator impedance, the static nature of VV-MPC and LVV-MPC schemes disturbs the tracking of the reference currents, especially at low-speed operating points (see Figure 18). However, the situation is completely different when the values of the stator parameters are higher. This fact is especially remarkable in the case of the q-current when more restrictive operating points are tested, as shown in Figure 18b. The usage of the dc-link voltage (IF4) in MV5-MPC limits its performance in this regard when the IM is characterized by high values of the stator inductance, as in 6PH-IM3 and 6PH-IM4. This undesired result is obtained even when the implementation of this technique involves a higher switching frequency in the VSC (see Figure 15). The suboptimal estimation of the variable application times also produces a notable tracking disturbance in the case of PULLA-MPC. This behavior can be identified in high operating points for 6PH-IM3 and 6PH-IM4 arrangements. As exposed in the previous section, the application time expressions of PULLA-MPC [24] and MV5-MPC [27] do not include the d-current values. This approach can provoke a notable tracking error for some stator parameter configurations. In addition, it is important to highlight that a more robust current tracking of static multi-vector solutions is obtained with a lower switching frequency. Therefore, it may be advisable to estimate these losses in order to select a more appropriate multi-vector solution for a specific electric drive.

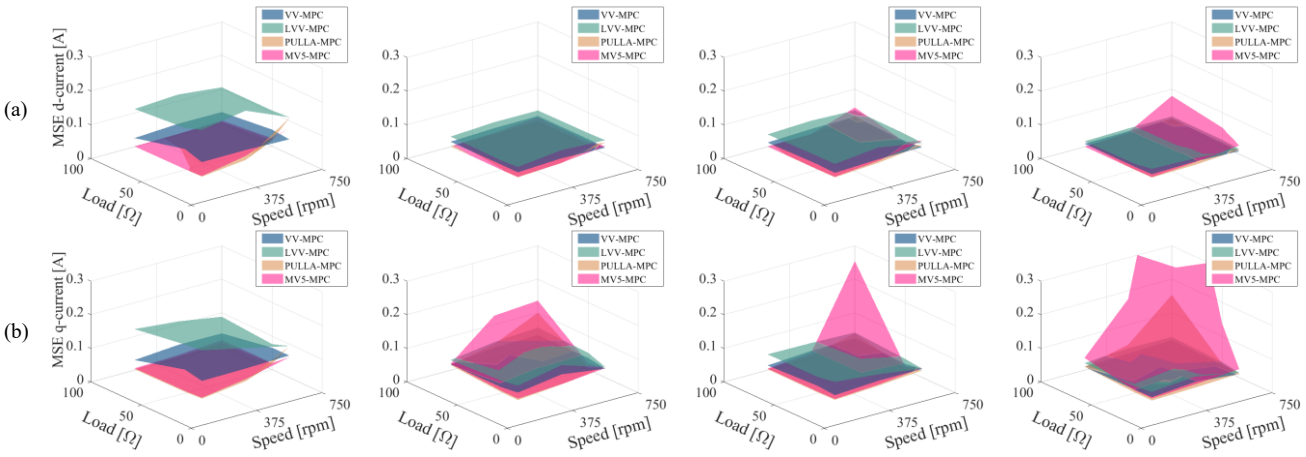


Figure 18. Selected indices for evaluating the current tracking in the experimental tests. (**a**) MSE *d* current and (**b**) MSE *q* current. From left column to right: 6PH-IM1, 6PH-IM2, 6PH-IM3 and 6PH-IM4.

5.2.3. Power Losses

Finally, the global losses generated to satisfy the operating points have been estimated and analyzed. In this regard, the VSC switching and conduction losses have been considered whereas, in the case of the IM, the stator copper losses have been valued. Figures 19 and 20 include the power losses determined in the experimental tests. Switching losses (Figure 19a) are directly related to the switching frequency and the RMS value of phase currents (see (20) and (21)). As is observed in Figure 15, the switching frequencies are lower when static multi-vector MPC schemes are implemented. Thus, they provide the lowest losses associated to the switching frequency, as depicted in Figure 19. In this respect, the LVV-MPC technique achieves the better response regardless of the stator configuration. As shown in Figure 19a, PULLA-MPC shows higher values than VV-MPC in a general manner and, unrelated to the employed multiphase drive, the MV5-MPC scheme reaches the higher switching losses (Figure 19a). The mentioned improvement in LVV-MPC is especially remarkable when high-speed and -torque conditions are explored. To evaluate the total electrical losses involved in the VSC, semiconductor conduction losses have also been determined. The expressions (23)–(25), obtained in [62], were employed for that goal. These conduction losses are strongly related with the RMS phase current values. For this reason, the VSC conduction losses show a similar behavior to the RMS current values (Figures 14b and 19b). Figure 19c shows that the switching loss impact is crucial in terms of the total VSC power losses. Consequently, the selection of a specific multi-vector solution involves a significant loss reduction for the analyzed electric drives.

In order to obtain a global view of the control performance, the stator copper losses have also been estimated for the studied operating conditions. These losses show a quadratic relation with the RMS of the phase currents. Observing Figure 20, it can be noted that the four types of multi-vector MPC schemes present slight variations in these types of losses. As expected, it can be observed that the stator copper losses increase in a remarkable manner when the IM is characterized by an augmented stator resistance (R_s). As shown in Figure 20, these power losses are the most significant among those taken into account in this assessment. A global view of the control performance can be obtained, for instance, observing Figures 18–20, since quantitative information about current tracking and power losses can be obtained for the considered multi-vector solutions operating in four different electric drives.

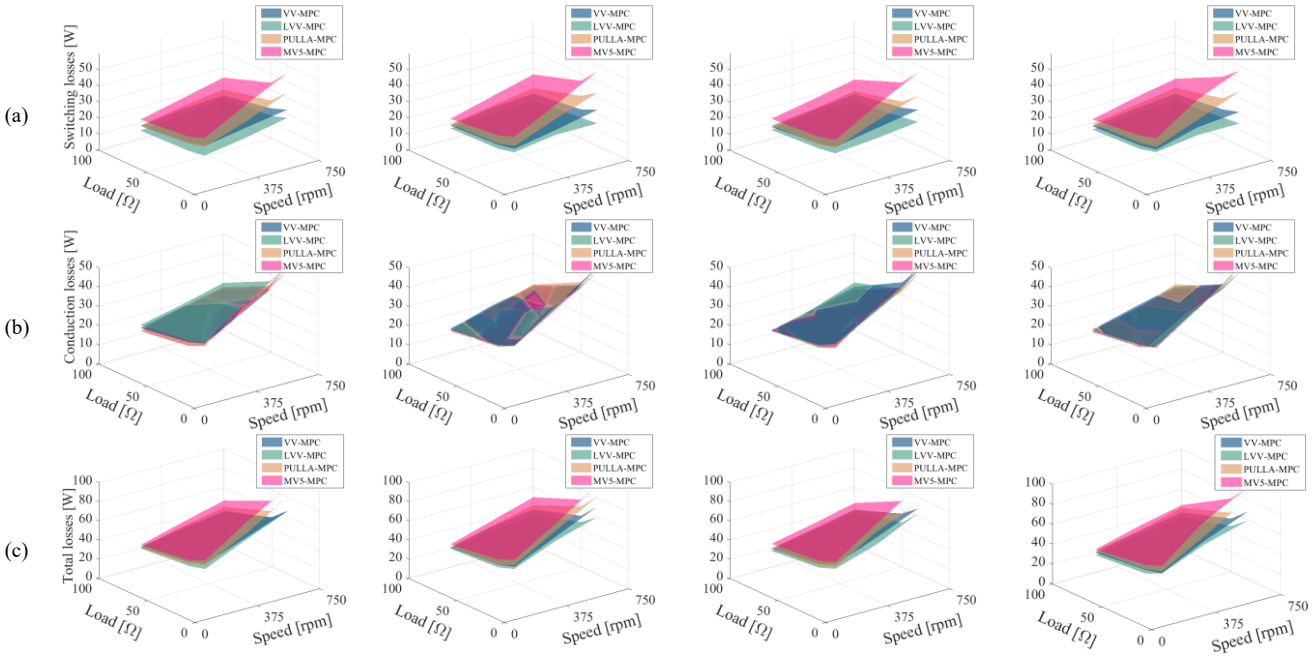


Figure 19. VSC power losses in the experimental tests. (**a**) Switching losses, (**b**) conduction losses and (**c**) VSC total losses. From left column to right: 6PH-IM1, 6PH-IM2, 6PH-IM3 and 6PH-IM4.

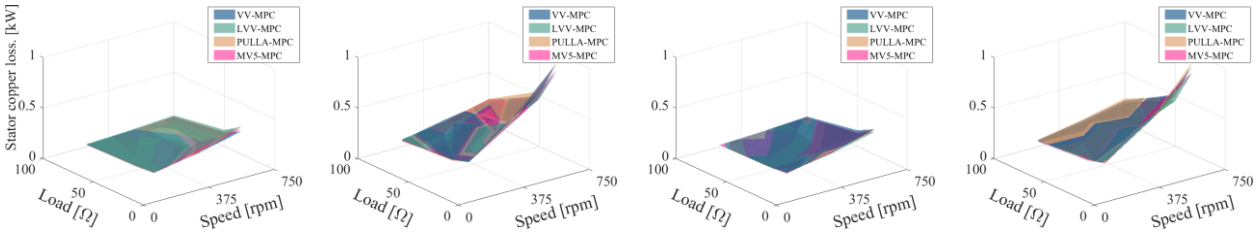


Figure 20. Stator copper losses in the experimental tests. From left column to right: 6PH-IM1, 6PH-IM2, 6PH-IM3 and 6PH-IM4.

To sum up the results from the different perspectives, Tables 4 and 5 provide a qualitative comparison of some aspects taken into account in this assessment. Specifically, Table 4 is concerned with the current quality and permits making a decision about what multi-vector control scheme can be employed from the perspective of the signal quality. Table 5 provides the same approach in consideration of the tracking of main components. The obtained results illustrate a significant dependence on the value of the considered stator parameters. It is worth highlighting that the best control strategy actually depends both on the machine parameters and the goals that are set by the control designer based on the operating conditions and application requirements. Consequently, the selection of the most appropriate regulation technique is not trivial since the choice involves a trade-off between different performance indices and there is not a universally valid option. The analysis provided in this study aims at guiding the most appropriate control approach by providing information about the different performances that can be obtained when the machine parameters, the control strategy or the operating point vary (shown in Figures 14–18 and briefly summarized in Tables 4 and 5). Since the machine parameters can be estimated in a simple manner in distributed winding machines [63,64], the control designer can obtain vital information for the design/selection task without the use of a complex process.

Table 4. Qualitative analysis of current waveform quality.

	6PH-IM1		6PH-IM2		6PH-IM3		6PH-IM4	
Scheme	**THD**	PtP_{xy}	**THD**	PtP_{xy}	**THD**	PtP_{xy}	**THD**	PtP_{xy}
VV-MPC	✗✗	✗✗	✗✗	✗✗	-	-	-	-
LVV-MPC	✗✗✗	✗✗✗	✗✗	✗✗	✗	✗	-	-
PULLA-MPC	✗	✗✗	✗	✗	-	✗	-	-
MV5-MPC	✓	✓	✓	✓	✓	✓	-	-

Table 5. Qualitative analysis of current tracking.

	6PH-IM1		6PH-IM2		6PH-IM3		6PH-IM4	
Scheme	**MSE** i_d	**MSE** i_q	**MSE** i_d	**MSE** i_q	**MSE** i_d	**MSE** i_q	**MSE** i_d	**MSE** i_q
VV-MPC	✗✗	✗✗	✗	✗	✓	✓	✓	✓
LVV-MPC	✗✗✗	✗✗	✗	✗	-	-	✓	✓
PULLA-MPC	✓	✓	✓	✗	✓	✗	✗	✗✗
MV5-MPC	✓	✓	✓	✗✗	✗	✗✗✗	✗✗	✗✗✗

6. Conclusions

Since standard MPC provides a poor current quality in multiphase machines with a low stator impedance, the use of multi-vector techniques has become popular as a means to enhance the steady-state performance. Nevertheless, the nature of such techniques is very different both from the point of view of the number of switching states (ranging from two to five) and the calculation of duties (using online and offline techniques). Similarly, each multi-vector approach has its own merits and shortcomings. Performance indices such as current tracking error, current distortion, switching frequency, utilization of the DC bus voltage or computational cost typically enter in conflict among themselves; hence, it becomes necessary to find a trade-off that may depend on the application context and requisites. The theoretical analysis and extensive experimental results obtained in this study allow for the extraction of some conclusions that may guide the control designers in the complex task of selecting the most suitable multi-vector MPC strategy. Some of these conclusions are listed hereafter, grouped into different items:

Item 1: Current quality

1. MV5 is the best choice when MPC is to be applied in machines with a low stator impedance. As a rule of thumb, in this scenario, the x-y plane becomes very sensitive and hence the use of multiple switching states and variable times of application is advantageous.
2. When the impedance of the stator becomes higher, the MPC strategies that use fewer voltage vectors (e.g., VV or LVV) can be more adequate since the THD becomes similar to MV5 but the switching frequency is reduced. It can be said that there is no mandatory need to use more switching states to satisfactorily reduce the value of the x-y currents.
3. The differences in the RMS values of phase currents are non-significant regardless of the implemented control scheme or the employed electric drive.

Item 2: Current tracking

1. The current tracking in both planes (x-y and $d-q$) is highly jeopardized when the control methods use a low number of switching states (e.g., VV and LVV) and the impedance of the stator is very low (e.g., 6PH-IM1). Consequently, MV5 or PULLA would be the best candidate in this case.
2. When the stator impedance is in the medium range (i.e., 6PH-IM3), the tracking error becomes much more similar to the different multi-vector strategies, and methods such as LVVs are more attractive because of their high utilization of the dc-link voltage and low switching frequency.

3. When the utilization of the dc-link voltage is reaching the limit, as may happen in machines like 6PH-IM4, the insufficient voltage generates an unacceptable current tracking; hence, methods such as MV5 should be avoided (unless the application only requires low-speed operation).

Item 3: Machine and VSC power losses

1. Switching losses are lower in static multi-vector MPC strategies (e.g., VV and LVV) and they do not depend on the stator parameters but on the number and types of voltage vectors that are applied in each sampling period.
2. Although Joule losses in the machine are dominant, the reduction in the switching losses in the case of LVV-MPC can be considered as an interesting benefit in high-speed/torque conditions.

It is worth noting in any case that the study does not aim to provide a fixed rule for selecting a control strategy but to give some guidelines and hints that may help the control designers to make a decision for their own application based on the control requirements. These can be characterized by a diverse nature, such as the range of operation, type of machine and converter, value of the stator impedance and dc-link voltage reserve, to name a few variables that will affect the final performance.

Supplementary Materials: The following supporting information can be downloaded at: https://www.mdpi.com/article/10.3390/machines12020115/s1.

Author Contributions: Conceptualization, I.G.-P., J.J.A. and M.J.D.; methodology, J.J.A. and I.G.-P.; software, J.J.A. and A.G.-P.; validation, J.J.A., I.G.-P. and M.J.D.; formal analysis, I.G.-P. and J.J.A.; investigation, J.J.A.; A.G.-P. and J.C.-R. resources, I.G.-P. and J.C.-R.; data curation, J.J.A., I.G.-P., A.G.-P., M.J.D. and J.C.-R.; writing—original draft preparation, J.J.A. and I.G.-P.; writing—review and editing, M.J.D.; visualization, J.J.A., A.G.-P. and J.C.-R.; supervision, J.J.A., I.G.-P. and M.J.D.; project administration, I.G.-P. and M.J.D.; funding acquisition, I.G.-P. and M.J.D. All authors have read and agreed to the published version of the manuscript.

Funding: This research was funded in part by the Spanish Government under the *Plan Estatal* with the reference PID2021-127131OB-I00, in part by *Proyectos Estratégicos Orientados a la Transición Ecológica y a la Transición Digital* under the reference TED2021-129558B-C21 and in part by the *Junta de Andalucia* under the reference UMA20-FEDERJA-039.

Data Availability Statement: Experimental data are provided as Supplementary Material.

Conflicts of Interest: The authors declare no conflicts of interest.

Appendix A

Predictive Machine Model Matrices

This section details the employed matrices in the discrete machine model of (4), which are:

$$[A] = \begin{bmatrix} a_{11} & a_{12} & 0 & 0 & a_{15} & a_{16} \\ a_{21} & a_{22} & 0 & 0 & a_{25} & a_{26} \\ 0 & 0 & a_{33} & 0 & 0 & 0 \\ 0 & 0 & 0 & a_{44} & 0 & 0 \\ a_{51} & a_{52} & 0 & 0 & a_{55} & a_{56} \\ a_{61} & a_{62} & 0 & 0 & a_{65} & a_{66} \end{bmatrix}, \tag{A1}$$

$$[B] = \begin{bmatrix} b_{11} & 0 & 0 & 0 \\ 0 & b_{22} & 0 & 0 \\ 0 & 0 & b_{33} & 0 \\ 0 & 0 & 0 & b_{44} \\ b_{51} & 0 & 0 & 0 \\ 0 & b_{62} & 0 & 0 \end{bmatrix}, \tag{A2}$$

and their coefficients are

$$\begin{array}{l} a_{11} = a_{22} = -\frac{R_s L_r}{L_s L_r - L_m^2}, a_{12} = -a_{21} = -\frac{L_m^2 \omega_r}{L_s L_r - L_m^2}, \\ a_{15} = a_{26} = \frac{R_s L_r}{L_s L_r - L_m^2}, a_{16} = -a_{25} = \frac{L_m L_r \omega_r}{L_s L_r - L_m^2}, \\ a_{33} = a_{44} = -\frac{R_s}{L_{ls}}, a_{51} = a_{62} = -\frac{R_s L_m}{L_s L_r - L_m^2}, \\ a_{52} = -a_{61} = -\frac{L_s L_m \omega_r}{L_s L_r - L_m^2}, a_{55} = a_{66} = \frac{R_r L_s}{L_s L_r - L_m^2}, \\ a_{56} = -a_{65} = -\frac{L_r L_s \omega_r}{L_s L_r - L_m^2}, b_{11} = b_{22} = \frac{L_r}{L_s L_r - L_m^2}, \\ b_{33} = b_{44} = \frac{1}{L_{ls}}, b_{51} = b_{62} = -\frac{L_m}{L_s L_r - L_m^2}. \end{array} \tag{A3}$$

where ω_r, L_r and L_s are the rotor angular speed, rotor inductance and stator inductance, respectively.

References

1. Levi, E. Multiphase Electric Machines for Variable-Speed Applications. *IEEE Trans. Ind. Electron.* **2008**, *55*, 1893–1909. [CrossRef]
2. Levi, E. Advances in Converter Control and Innovative Exploitation of Additional Degrees of Freedom for Multiphase Machines. *IEEE Trans. Ind. Electron.* **2016**, *63*, 433–448. [CrossRef]
3. Lu, H.; Li, J.; Qu, R.; Ye, D. Fault-tolerant predictive current control with two-vector modulation for six-phase permanent magnet synchronous machine drives. *IET Electr. Power Appl.* **2018**, *12*, 169–178. [CrossRef]
4. Lu, H.; Li, J.; Qu, R.; Ye, D.; Lu, Y. Fault-Tolerant Predictive Control of Six-Phase PMSM Drives Based on Pulsewidth Modulation. *IEEE Trans. Ind. Electron.* **2019**, *66*, 4992–5003. [CrossRef]
5. Moraes, T.J.D.S.; Nguyen, N.K.; Semail, E.; Meinguet, F.; Guerin, M. Dual-Multiphase Motor Drives for Fault-Tolerant Applications: Power Electronic Structures and Control Strategies. *IEEE Trans. Power Electron.* **2018**, *33*, 572–580. [CrossRef]
6. Abad, H.B.B.; Ojaghi, M.; Taheri, A. Extra Freedom Degrees of Six-Phase Induction Motors Used to Diagnose Stator Inter-Turn Faults. *Electr. Power Components Syst.* **2021**, *49*, 294–307. [CrossRef]
7. Levi, E.; Jones, M.; Vukosavic, S.N. A series-connected two-motor six-phase drive with induction and permanent magnet machines. *IEEE Trans. Energy Convers.* **2006**, *21*, 121–129. [CrossRef]
8. Levi, E.; Jones, M.; N.Vukosavic, S.; Toliyat, H.A. A novel concept of a multiphase, multimotor vector controlled drive system supplied from a single voltage source inverter. *IEEE Trans. Power Electron.* **2004**, *19*, 320–335. [CrossRef]
9. Blaschke, F. The principle of field-orientation as applied to the new transvector closed-loop control system for rotating machine. *Siemens Rev.* **1972**, *39*, 217–220.
10. Singh, G.K.; Nam, K.; Lim, S.K. A simple indirect field-oriented control scheme for multiphase induction machine. *IEEE Trans. Ind. Electron.* **2005**, *52*, 1177–1184. [CrossRef]
11. Yepes, A.G.; Gandoy, J.D.; Toliyat, H.A. Improvement in DC-Link Utilization with Reduced Current and Torque Deterioration for Five-Phase Drives by Combination of Circulating-Current Filters and Simple Carrier-Based PWM Based on Closed-Form Expressions. *IEEE Trans. Ind. Electron.* **2021**, *68*, 960–971. [CrossRef]
12. Robles, E.; Fernandez, M.; Andreu, J.; Ibarra, E.; Zaragoza, J.; Ugalde, U. Common-mode voltage mitigation in multiphase electric motor drive systems. *Renew. Sustain. Energy Rev.* **2022**, *157*, 111971. [CrossRef]
13. Levi, E.; Bojoi, R.; Profumo, F.; Toliyat, H.A.; Williamson, S. Multiphase induction motor drives—A technology status review. *IET Electr. Power Appl.* **2007**, *1*, 489–516. [CrossRef]
14. Hava, A.; Kerkman, R.; Lipo, T. Carrier-based PWM-VSI overmodulation strategies: Analysis, comparison, and design. *IEEE Trans. Power Electron.* **1998**, *13*, 674–689. [CrossRef]
15. Lopez, O.; Alvarez, J.; Yepes, A.G.; Baneira, F.; Perez-Estevez, D.; Freijedo, F.D.; Doval-Gandoy, J. Carrier-Based PWM Equivalent to Multilevel Multiphase Space Vector PWM Techniques. *IEEE Trans. Ind. Electron.* **2020**, *67*, 5220–5231. [CrossRef]
16. Holmes, G.; Lipo, T.; Lipo, T. *Pulse Width Modulation for Power Converters: Principles and Practice*; Wiley: Hoboken, NJ, USA, 2003.
17. Carrasco, G.; Silva, C.A. Space Vector PWM Method for Five-Phase Two-Level VSI with Minimum Harmonic Injection in the Overmodulation Region. *IEEE Trans. Ind. Electron.* **2013**, *60*, 2042–2053. [CrossRef]
18. Lim, C.S.; Levi, E.; Jones, M.; Rahim, N.A.; Hew, W.P. FCS-MPC-Based Current Control of a Five-Phase Induction Motor and its Comparison with PI-PWM Control. *EEE Trans. Ind. Electron.* **2014**, *61*, 149–163. [CrossRef]

19. Arahal, M.; Satue, M.G.; Barrero, F.; Ortega, M.G. Adaptive Cost Function FCSMPC for 6-Phase IMs. *Energies* **2021**, *14*, 52222. [CrossRef]
20. Bhowate, A.; Aware, M.; Sharma, S.; Tatte, Y. Predictive Torque Control for Five Phase Induction Motor Drive with Common Mode Voltage Reduction. In Proceedings of the International Power Electronics Conference, Niigata, Japan, 20–24 May 2018; pp. 1730–1735. [CrossRef]
21. Luo, Y.; Liu, C. Multi-Vector-Based Model Predictive Torque Control for a Six-Phase PMSM Motor with Fixed Switching Frequency. *IEEE Trans. Energy Convers.* **2019**, *34*, 1369–1379. [CrossRef]
22. Xue, C.; Song, W.; Feng, X. Finite control-set model predictive current control of five-phase permanent-magnet synchronous machine based on virtual voltage vectors. *IET Electr. Power Appl.* **2017**, *11*, 836–846. [CrossRef]
23. Gonzalez-Prieto, A.; Gonzalez-Prieto, I.; Duran, M.J.; Aciego, J.J.; Salas-Biedma, P. Current Harmonic Mitigation Using a Multi-Vector Solution for MPC in Six-Phase Electric Drives. *IEEE Access* **2021**, *9*, 117761–117771. [CrossRef]
24. Duran, M.; Gonzalez-Prieto, I.; Prieto, A.G.; Carrillo-Rios, J.; Aciego, J.J.; Salas-Biedma, P. Proportional Usage of Low-Level Actions in Model Predictive Control for Six-Phase Electric Drives. *Energies* **2021**, *14*, 4358. [CrossRef]
25. Duran, M.J.; Gonzalez-Prieto, I.; Gonzalez-Prieto, A. Large virtual voltage vectors for direct controllers in six-phase electric drives. *Int. J. Electr. Power Energy Syst.* **2021**, *125*, 106425. [CrossRef]
26. Gonzalez-Prieto, I.; Duran, M.J.; Aciego, J.J.; Martin, C.; Barrero, F. Model Predictive Control of Six-Phase Induction Motor Drives Using Virtual Voltage Vectors. *IEEE Trans. Ind. Electron.* **2018**, *65*, 27–37. [CrossRef]
27. Duran, M.; Gonzalez-Prieto, I.; Gonzalez-Prieto, A.; Aciego, J.J. The Evolution of Model Predictive Control in Multiphase Electric Drives: A Growing Field of Research. *IEEE Ind. Electron. Mag.* **2022**, *16*, 29–39. [CrossRef]
28. Goncalves, P.; Cruz, S.; Mendes, A. Multistage Predictive Current Control Based on Virtual Vectors for the Reduction of Current Harmonics in Six-Phase PMSMs. *IEEE Trans. Energy Convers.* **2021**, *36*, 1368–1377. [CrossRef]
29. Tao, T.; Zhao, W.; He, Y.; Zhu, J.; Tan, H.; Xue, R. Multivector Predictive Current Control for Five-Phase PM Motor by Using Hybrid Duty Modulation Technology. *IEEE Trans. Transp. Electrif.* **2020**, *6*, 1603–1612. [CrossRef]
30. Ayala, M.; Doval-Gandoy, J.; Rodas, J.; Gonzalez, O.; Gregor, R.; Rivera, M. A Novel Modulated Model Predictive Control Applied to Six-Phase Induction Motor Drives. *IEEE Trans. Ind. Electron.* **2021**, *68*, 3672–3682. [CrossRef]
31. Yu, B.; Song, W.; Feng, J. Virtual Voltage Vector-Based Model Predictive Current Control for Five-Phase VSIs with Common-Mode Voltage Reduction. *IEEE Trans. Transp. Electrif.* **2021**, *7*, 706–717. [CrossRef]
32. Goncalves, P.; Cruz, S.M.A.; Mendes, A.M.S. Bi-subspace predictive current control of six-phase PMSM drives based on virtual vectors with optimal amplitude. *IET Electr. Power Appl.* **2019**, *13*, 1672–1683. [CrossRef]
33. Arahal, M.R.; Satue, M.G.; Barrero, F.; Martin, C. Online Adaptive Set of Virtual Voltage Vectors for Stator Current Regulation of a Six-Phase Induction Machine Using Finite State Model Predictive Controllers. *Appl. Sci.* **2023**, *13*, 4113. [CrossRef]
34. Xue, Z.; Niu, S.; Chau, A.M.H.; Luo, Y.; Lin, H.; Li, X. Recent Advances in Multi-Phase Electric Drives Model Predictive Control in Renewable Energy Application: A State-of-the-Art Review. *World Electr. Veh. J.* **2023**, *14*. [CrossRef]
35. Frikha, M.A.; Croonen, J.; Deepak, K.; Benomar, Y.; Baghdadi, M.; Hegazy, O. Multiphase Motors and Drive Systems for Electric Vehicle Powertrains: State of the Art Analysis and Future Trends. *Energies* **2023**, *16*, 45. [CrossRef]
36. Ehsani, M.; Singh, K.V.; Bansal, H.O.; Mehrjardi, R.T. State of the Art and Trends in Electric and Hybrid Electric Vehicles. *Proc. IEEE* **2021**, *109*, 967–984. [CrossRef]
37. Ahmed, A.A.; Koh, B.K.; Lee, Y.I. A Comparison of Finite Control Set and Continuous Control Set Model Predictive Control Schemes for Speed Control of Induction Motors. *IEEE Trans. Ind. Inform.* **2018**, *14*, 1334–1346. [CrossRef]
38. Xue, C.; Song, W.; Wu, X.; Feng, X. A Constant Switching Frequency Finite-Control-Set Predictive Current Control Scheme of a Five-Phase Inverter with Duty-Ratio Optimization. *IEEE Trans. Power Electron.* **2018**, *33*, 3583–3594. [CrossRef]
39. Luo, Y.; Liu, C. A Simplified Model Predictive Control for a Dual Three-Phase PMSM with Reduced Harmonic Currents. *IEEE Trans. Ind. Electron.* **2018**, *65*, 9079–9089. [CrossRef]
40. Liu, Z.; Li, Y.; Zheng, Z. A review of drive techniques for multiphase machines. *CES Trans. Electr. Mach. Syst.* **2018**, *2*, 243–251. [CrossRef]
41. Liu, S.; Liu, C. Virtual-vector-based robust predictive current control for dual three-phase PMSM. *IEEE Trans. Ind. Electron.* **2021**, *68*, 2048–2058. [CrossRef]
42. Martin, C.; Bermudez, M.; Barrero, F.; Arahal, M.R.; Kestelyn, X.; Duran, J. Sensitivity of predictive controllers to parameter variation in five-phase induction motor drives. *Control Eng. Pract.* **2017**, *68*, 23–31. [CrossRef]
43. Bogado, B.; Barrero, F.; Arahal, M.R.; Toral, S.; Levi, E. Sensitivity to electrical parameter variations of Predictive Current Control in multiphase drives. In Proceedings of the IECON 2013—39th Annual Conference of the IEEE Industrial Electronics Society, Vienna, Austria, 10–13 November 2013; pp. 5215–5220. [CrossRef]
44. Guo, L.; Chen, M.; Li, Y.; Wang, P.; Jin, N.; Wu, J. Hybrid Multi-Vector Modulated Model Predictive Control Strategy for Voltage Source Inverters Based on a New Visualization Analysis Method. *IEEE Trans. Transp. Electrif.* **2023**, *9*, 8–21. [CrossRef]
45. Sun, J.; Yang, Y.; Chen, R.; Zhang, X.; Lim, C.S.; Rodriguez, J. An efficient multi-vector based model predictive current control for PMSM drive. *CPSS Trans. Power Electron. Appl.* **2023**, 1–11. [CrossRef]
46. Yang, Y.; Wen, H.; Fan, M.; He, L.; Xie, M.; Chen, R.; Norambuena, M.; Rodriguez, J. Multiple-Voltage-Vector Model Predictive Control with Reduced Complexity for Multilevel Inverters. *IEEE Trans. Transp. Electrif.* **2020**, *6*, 105–117. [CrossRef]

47. Deng, W.; Zhang, Q.; Xie, W. An Enhanced Virtual Vector-Based Model Predictive Control for PMSM Drives to Reduce Common-Mode Voltage Considering Dead Time Effect. *IEEE J. Emerg. Sel. Top. Power Electron.* **2023**, *11*, 4659–4668. [CrossRef]
48. Che, H.S.; Levi, E.; Jones, M.; Hew, W.P.; Rahim, N.A. Current control methods for an asymmetrical six-phase induction motor drive. *IEEE Trans. Power Electron.* **2014**, *29*, 407–417. [CrossRef]
49. Wang, H.; Wu, X.; Zheng, X.; Yuan, X. Virtual Voltage Vector Based Model Predictive Control for a Nine-Phase Open-End Winding PMSM with a Common DC Bus. *IEEE Trans. Ind. Electron.* **2022**, *69*, 5386–5397. [CrossRef]
50. Gonzalez, J.O.; Perez-Estevez, D.; R. Wu, J.D.G.; Mawby, P.; Alatise, O. Power Device Losses in Two-Level Converters with Direct Current Controllers for Grid Connected Applications. In Proceedings of the 2021 IEEE Energy Conversion Congress and Exposition (ECCE), Vancouver, BC, Canada, 10–14 October 2021; pp. 3154–3159. [CrossRef]
51. Zhao, Y.; Lipo, T.A. Space vector PWM control of dual three-phase induction machine using vector space decomposition. *IEEE Trans. Ind. Appl.* **1995**, *31*, 1100–1109. [CrossRef]
52. Goncalves, P.; Cruz, S.; Mendes, A. Finite Control Set Model Predictive Control of Six-Phase Asymmetrical Machines—An Overview. *Energies* **2019**, *12*, 4693. [CrossRef]
53. Xu, Z.; Wang, Z.; Wang, X.; Cheng, M. Predictive current control method for dual three-phase PMSM drives with reduced switching frequency and low-computation burden. *IET Electr. Power Appl.* **2020**, *14*, 668–677. [CrossRef]
54. Yang, G.; Hussain, H.; Li, S.; Zhang, X.; Yang, J.; Lee, C.H.T. Design and Analysis of Universal Natural Fault-Tolerant SVPWM Strategy with Simplified Fault Diagnosis for Multiphase Motor Drives. *IEEE J. Emerg. Sel. Top. Power Electron.* **2023**, *11*, 4340–4354. [CrossRef]
55. Wang, H.; Wu, X.; Zheng, X.; Yuan, X. Model Predictive Current Control of Nine-Phase Open-End Winding PMSMs with an Online Virtual Vector Synthesis Strategy. *IEEE Trans. Ind. Electron.* **2023**, *70*, 2199–2208. [CrossRef]
56. Kindl, V.; Cermak, R.; Ferkova, Z.; Skala, B. Review of Time and Space Harmonics in Multi-Phase Induction Machine. *Energies* **2020**, *13*, 496. [CrossRef]
57. Abdel-Khalik, A.S.; Abdel-Majeed, M.S.; Ahmed, S. Effect of Winding Configuration on Six-Phase Induction Machine Parameters and Performance. *IEEE Access* **2020**, *8*, 223009–223020. [CrossRef]
58. Rodriguez, J.; Garcia, C.; Mora, A.; Davari, S.A.; Rodas, J.; Valencia, D.F.; Elmorshedy, M.; Wang, F.; Zuo, K.; Tarisciotti, L.; et al. Latest Advances of Model Predictive Control in Electrical Drives-Part II: Applications and Benchmarking with Classical Control Methods. *IEEE Trans. Power Electron.* **2022**, *37*, 5047–5061. [CrossRef]
59. Che, H.S.; Hew, W.P. Dual three-phase operation of single neutral symmetrical six-phase machine for improved performance. In Proceedings of the IECON 2015—41st Annual Conference of the IEEE Industrial Electronics Society, Yokohama, Japan, 9–12 November 2015; pp. 001176–001181. [CrossRef]
60. Yepes, A.G.; Doval-Gandoy, J.; Baneira, F.; Toliyat, H.A. Comparison of stator winding connections in multiphase drives under healthy operation and with one open converter leg. *IET Electr. Power Appl.* **2020**, *14*, 584–596. [CrossRef]
61. Shawier, A.; Habib, A.; Mamdouh, M.; Abdel-Khalik, A.S.; Ahmed, K.H. Assessment of Predictive Current Control of Six-Phase Induction Motor with Different Winding Configurations. *IEEE Access* **2021**, *9*, 81125–81138. [CrossRef]
62. Hafezi, H.; Faranda, R. A New Approach for Power Losses Evaluation of IGBT/Diode Module. *Electronics* **2021**, *10*, 280. [CrossRef]
63. Yepes, A.G.; Riveros, J.A.; Doval-Gandoy, J.; Barrero, F.; Lopez, ÃŞ.; Bogado, B.; Jones, M.; Levi, E. Parameter Identification of Multiphase Induction Machines with Distributed Windings—Part 1: Sinusoidal Excitation Methods. *IEEE Trans. Energy Convers.* **2012**, *27*, 1056–1066. [CrossRef]
64. Riveros, J.A.; Yepes, A.G.; Barrero, F.; Doval-Gandoy, J.; Bogado, B.; Lopez, O.; Jones, M.; Levi, E. Parameter Identification of Multiphase Induction Machines with Distributed Windings—Part 2: Time-Domain Techniques. *IEEE Trans. Energy Convers.* **2012**, *27*, 1067–1077. [CrossRef]

Disclaimer/Publisher's Note: The statements, opinions and data contained in all publications are solely those of the individual author(s) and contributor(s) and not of MDPI and/or the editor(s). MDPI and/or the editor(s) disclaim responsibility for any injury to people or property resulting from any ideas, methods, instructions or products referred to in the content.